Immature olfactory sensory neurons provide behaviorally useful sensory input to the olfactory bulb

Authors and Affiliations

Jane S. Huang[1], Tenzin Kunkhyen[1], Beichen Liu[1,2], Ryan J. Muggleton[1,2], Jonathan T. Avon[1] and Claire E.J. Cheetham[1,2]

[1] Department of Neurobiology, University of Pittsburgh, 200 Lothrop St, Pittsburgh PA 15232

[2] Department of Biological Sciences, Carnegie Mellon University, 4400 Fifth Avenue, Pittsburgh PA 15213

Contact Info

Correspondence: cheetham@pitt.edu

Abstract

Postnatal neurogenesis provides an opportunity to understand how newborn neurons functionally integrate into circuits to restore lost function. Newborn olfactory sensory neurons (OSNs) wire into highly organized olfactory bulb (OB) circuits throughout life, enabling lifelong plasticity and regeneration. Immature OSNs can form functional synapses capable of evoking firing in OB projection neurons. However, what contribution, if any, immature OSNs make to odor processing is unknown. Indeed, because immature OSNs can express multiple odorant receptors, any input that they do provide could degrade the odorant selectivity of input to OB glomeruli. Here, we used a combination of *in vivo* 2-photon calcium imaging, optogenetics, electrophysiology and behavioral assays to show that immature OSNs provide odor input to the OB, where they form monosynaptic connections with excitatory neurons. Importantly, immature OSNs responded as selectively to odorants as mature OSNs. Furthermore, mice successfully performed odor detection tasks using sensory input from immature OSNs alone. Immature OSNs responded more strongly to low odorant concentrations but their responses were less concentration dependent than those of mature OSNs, suggesting that immature and mature OSNs provide distinct odor input streams to each glomerulus. Together, our findings suggest that sensory input mediated by immature OSNs plays a previously unappreciated role in olfactory-guided behavior.

Introduction

Most mammalian neurons are generated during embryonic or early postnatal life and cannot be replaced if they are damaged or lost. In contrast, newborn neurons in the olfactory system continue to be generated and wire successfully into highly ordered circuits throughout life (Graziadei and Graziadei, 1978; Lois and Alvarez-Buylla, 1993; Luskin, 1993). This endows the olfactory bulb (OB) with a high level of lifelong plasticity (Cheetham et al., 2016; Forest et al., 2019; Grelat et al., 2018; Li et al., 2018; Lledo et al., 2006; Wallace et al., 2017) and enables substantial functional recovery after injury (Blanco-Hernández et al., 2012; Cheung et al., 2014; Kikuta et al., 2015; Schwob et al., 1999). Combined with its optical accessibility, the mouse OB hence provides a unique opportunity to understand how endogenously generated stem cell-derived neurons functionally integrate into established circuits.

One of these postnatally generated populations, the olfactory sensory neurons (OSNs), provides odor input to the OB (Firestein, 2001). In all terrestrial mammals including humans, newborn OSNs are generated throughout life from basal stem cells in the olfactory epithelium (OE) (Graziadei and Graziadei, 1978; Hahn et al., 2005; Kondo et al., 2010). OSNs have a finite lifespan: in mice, their half-life is approximately one month, with most surviving for less than three months except under filtered air or pathogen-free conditions (Hinds et al., 1984; Holl, 2018; Mackay-Sim and Kittel, 1991). OSN neurogenesis is also upregulated following chemical, mechanical or virus-mediated damage to the OE, enabling rapid repopulation even after an almost complete loss of OSNs (Kikuta et al., 2015; Leung et al., 2007; Schwob et al., 1999). Furthermore, regeneration of sensory input to the OB enables significant functional recovery of odor representations and olfactory-guided behavior within 6-12 weeks (Blanco-Hernández et al., 2012; Cheung et al., 2014). Hence, newborn OSNs in both the healthy and the regenerating OE face the challenge of wiring into pre-existing circuits to maintain or restore function, rather than disrupt it. Determining how this is achieved has broad implications both for understanding how functional integration of stem cell-derived neurons can be promoted to repair damage in other brain regions, and for the treatment

of anosmia, which can lead to depression and poor nutrition (Doty and Kamath, 2014; Kohli et al., 2016).

Individual OSNs follow a well-defined developmental pathway. After terminal division of OE basal cells, Ascl1-expressing neuronally-committed intermediate cells briefly become nascent OSNs that express CXCR4 and DBN1 before transitioning to GAP43- and Gγ8-expressing immature OSNs (McIntyre et al., 2010; Ryba and Tirindelli, 1995; Schwob et al., 2017; Verhaagen et al., 1989). OSNs begin to express olfactory marker protein (OMP) and downregulate GAP43 expression 7-8 days after terminal cell division (Liberia et al., 2019; Miragall and Graziadei, 1982; Rodriguez-Gil et al., 2015; Savya et al., 2019). Mature OSNs express OMP but not GAP43 or Gγ8. Each mature OSN also typically expresses a single odorant receptor (OR) allele (Chess et al., 1994; Hanchate et al., 2015; Saraiva et al., 2015; Serizawa et al., 2000, 2003), selected from a repertoire of approximately 1100 functional receptors (Clowney et al., 2011). The expressed OR determines both the odorant selectivity of the mature OSN (Bozza et al., 2002; Dalton and Lomvardas, 2014; Malnic et al., 1999) and the glomerulus to which it projects its axon (Bozza et al., 2002; Feinstein and Mombaerts, 2004; Wang et al., 1998). This generates a highly ordered map of odor input to the brain.

In contrast to mature OSNs, whether immature OSNs respond to odorants is unknown. OSNs begin to express ORs just 4 days after terminal cell division, several days before they express OMP (Rodriguez-Gil et al., 2015). Furthermore, a subset of immature OSNs express transcripts that encode both ORs and the molecular machinery necessary to transduce odorant binding into action potentials (Hanchate et al., 2015). This suggests that immature OSNs may be capable of odorant binding and signal transduction. We have also shown previously that immature Gγ8-expressing OSNs form synapses with OB neurons in the glomerular layer and that optogenetic stimulation of immature OSN axons evokes robust firing in OB neurons in the glomerular, external plexiform and mitral cell layers (Cheetham et al., 2016). Hence, if immature OSNs can detect and transduce odorant binding, then they may play a previously unknown role in transmitting odor information to OB neurons to support olfactory-guided behavior. However, this would also

raise an important question: is input from immature OSNs odorant selective? Recent studies have shown that a subset of immature OSNs express transcripts encoding multiple ORs (Hanchate et al., 2015; Tan et al., 2015). Therefore, if multi-OR expressing immature OSNs were to provide odor information to the OB, they could degrade the odorant selectivity of glomerular input.

Determining what contribution, if any, immature OSNs make to OB sensory input is essential in understanding both how odor information is processed by OB circuits and how adult-born OSNs continue to wire into highly ordered circuits without disrupting existing function. Here, we use *in vivo* 2-photon calcium imaging to demonstrate that immature OSNs provide input to glomeruli that is as odorant selective as that provided by mature OSNs. However, immature OSNs encode concentration less strongly than their mature counterparts. We also show using optogenetic stimulation that immature OSNs form monosynaptic connections with excitatory OB neurons. Furthermore, we demonstrate that sensory input from immature OSNs is sufficient to mediate odor detection and simple odor discrimination in behavioral tasks.

Results

Immature OSNs respond as selectively as mature OSNs to odorants

To determine whether immature OSNs can detect and transduce odorant binding, we bred Gγ8-tTA;tetO-GCaMP6s (referred to as Gγ8-GCaMP6s) mice, in which immature OSNs selectively express the genetically encoded calcium indicator GCaMP6s (Fig. 1A,B). Unlike recombinase-based expression systems, the tetracycline transactivator system enables transient expression of a reporter protein during a particular developmental stage. We validated the specificity of GCaMP6s expression in immature OSNs in 3-week-old mice, a time point at which large numbers of immature OSNs are present in the OE (Tirindelli and Ryba, 1996). Only 3% of Gγ8-GCaMP6s-expressing neurons also expressed OMP (Fig. 1B,C). Hence, the vast majority of Gγ8-GCaMP6s-expressing OSNs are immature GCaMP6s+OMP- neurons, whereas a very small proportion of GCaMP6s+OMP+ OSNs are in transition to maturity (Cheetham et al., 2016).

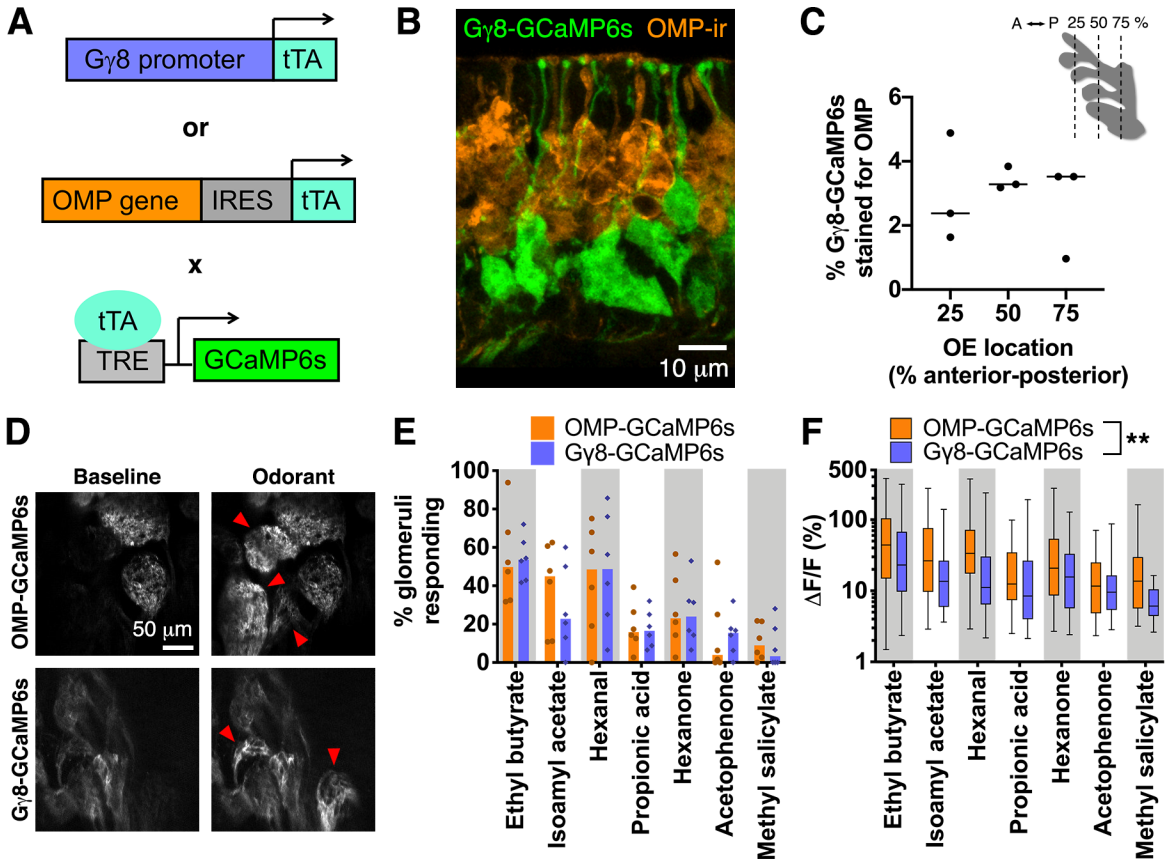

Figure 1. Immature OSNs can detect and transduce odorants.
A. Schematic of breeding strategy to generate mice expressing GCaMP6s in either immature or mature OSNs under control of the Gγ8 or OMP promoter, respectively, using the tetracycline transactivator system. **B.** Maximum intensity projection of confocal z-stack of coronal OE section from a Gγ8-GCaMP6s mouse showing lack of colocalization with OMP-stained OSNs. **C.** Co-expression of OMP in Gγ8-GCaMP6s-expressing OSNs in the septal OE along the anterior-posterior axis. Only 3.0 ± 1.2 % of Gγ8-GCaMP6s-expressing neurons co-express OMP (mean ± s.d., n = 4118 Gγ8-GCaMP6s-expressing OSNs from 3 mice). Inset shows location of analyzed OE sections. **D.** Example 2-photon images of single z-plane during single trial showing baseline fluorescence and odorant-evoked responses in OMP-GCaMP6s and Gγ8-GCaMP6s mice. Red arrows indicate ethyl butyrate-responsive glomeruli. **E.** A similar percentage of glomeruli respond to each of the 7 odorants in Gγ8-GCaMP6s vs. OMP-GCaMP6s mice (Wilcoxon signed rank test. P = 0.47, W = -10, n = 6 mice per group). Colored bars: median of 6 mice per group, symbols: values for individual mice. Gray shaded areas are shown to aid visualisation only. **F.** Odorant-evoked responses are larger in amplitude in OMP-GCaMP6s mice vs. Gγ8-GCaMP6s mice (Two-way ANOVA. Effect of genotype: P = 0.003, $F_{1,568}$ = 8.87. Effect of odorant: P < 0.001, $F_{6,568}$ = 7.42. Interaction: P = 0.36, $F_{6,568}$ = 1.10. n = 21-87 responding glomeruli per odorant for OMP-GCaMP6s and 16-78 responding glomeruli per odorant for Gγ8-GCaMP6s). Boxes: quartiles. Whiskers: range.

We then implanted acute cranial windows over the OB of 3-week-old Gγ8-GCaMP6s mice and performed 2-photon calcium imaging of glomeruli innervated by immature OSN axons in response to stimulation with a panel of seven dorsal OB-activating odorants. All responses were blank stimulus-subtracted to account for any potential mechanosensory contribution to evoked responses as a result of changes in air flow (Fig. 1D) (Carey et al.,

2009; Chen et al., 2012; Connelly et al., 2015; Grosmaitre et al., 2007; Iwata et al., 2017). We found that immature OSN axons in many glomeruli responded to at least one odorant in the panel (Fig. 1E). Indeed, across the population of imaged glomeruli, the proportion that responded to each odorant in Gγ8-GCaMP6s mice was similar to that in OMP-GCaMP6s mice, in which GCaMP6s is expressed in mature OSNs (Fig. 1A,E). However, odorant-evoked response amplitudes were smaller in glomeruli in Gγ8-GCaMP6s mice than in OMP-GCaMP6s mice across the odor panel (Fig. 1F). These data provide the first evidence that immature OSNs can detect and transduce odorant binding to generate action potentials that propagate to the OB, resulting in calcium influx at glomerular axon terminals.

Recent studies have suggested that mature OSNs can respond to mechanical stimuli using the same signal transduction machinery as for odor input (Carey et al., 2009; Chen et al., 2012; Connelly et al., 2015; Grosmaitre et al., 2007; Iwata et al., 2017). We found that a deodorized air puff stimulus delivered to the external nares elicited putative mechanosensory responses in a similar proportion of glomeruli in Gγ8-GCaMP6s and OMP-GCaMP6s mice (Fig. S1A,B). The amplitude of air puff responses was also similar for glomeruli in Gγ8-GCaMP6s and OMP-GCaMP6s mice (Fig. S1C). Both the proportion of responding glomeruli (Fig. S1B) and the amplitude of air puff-induced glomerular responses (Fig. S1C) were similar to a previous report of mechanosensory responses induced by increased air flow (Iwata et al., 2017). Together, these data provide evidence for putative mechanosensory responses in immature OSNs.

Some immature OSNs express transcripts encoding multiple ORs (Hanchate et al., 2015; Tan et al., 2015). In particular, one study showed that some “late immature” OSNs, which already express transcripts encoding all of the essential olfactory signal transduction machinery, still express multiple OR transcripts (Hanchate et al., 2015). If this is also the case at the protein level, immature OSNs innervating each glomerulus may respond to a wider range of odorants. Therefore, we compared the selectivity of odorant responses in individual glomeruli in Gγ8-GCaMP6s and OMP-GCaMP6s mice. We found that the number of odorants to which an individual glomerulus responded was similar in Gγ8-

GCaMP6s and OMP-GCaMP6s mice (Fig. 2A). However, it is possible that selectivity is also reflected in response magnitude, with mature OSNs responding more strongly to a smaller number of odorants, while immature OSN axons innervating glomeruli may respond more similarly to multiple odorants. Indeed, the smaller odorant-evoked response amplitudes in Gγ8-GCaMP6s mice (Fig. 1F) support this possibility. Therefore, we also evaluated odorant selectivity by calculating the lifetime sparseness (S_L) (Poo and Isaacson, 2009) of glomerular odorant responses. S_L provides a measure of the breadth of odor tuning that accounts for the amplitude of odorant-evoked responses: a glomerulus with $S_L = 0$ responds equally to all seven odorants whereas a glomerulus with $S_L = 1$ responds to a single odorant. We found that S_L was similar in Gγ8-GCaMP6s and OMP-GCaMP6s mice, with most glomeruli responding to a small number of odorants in the panel (Fig. 2B). Hence, odorant selectivity was equivalent in Gγ8-GCaMP6s and OMP-GCaMP6s mice.

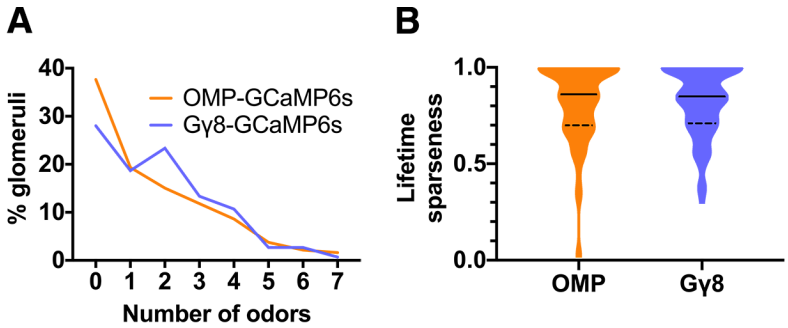

Figure 2. Immature and mature OSN axons show equivalent odorant selectivity.
A. Glomeruli in OMP-GCaMP6s and Gγ8-GCaMP6s mice respond to a similar number of odorants in a seven-odorant panel (Wilcoxon signed rank test: P = 0.95, W = -2, n = 186 glomeruli in 6 OMP-GCaMP6s mice and 150 glomeruli in 6 Gγ8-GCaMP6s mice). **B.** Violin plot showing similar lifetime sparseness of glomerular odorant responses in Gγ8-GCaMP6s and OMP-GCaMP6s mice (Kolmogorov-Smirnov test: P = 1.00, D = 0.049. n = 120 responding glomeruli in 6 OMP-GCaMP6s mice and 97 responding glomeruli in 6 Gγ8-GCaMP6s mice). Solid lines: median. Dashed lines: quartiles. Upper quartiles are at 1 and so not shown.

Differential concentration coding in immature and mature OSNs

Previous studies have shown that increased odorant concentration results in the activation of additional glomeruli (Johnson and Leon, 2000; Meister and Bonhoeffer, 2001; Rubin and Katz, 1999; Wachowiak and Cohen, 2001). Consistent with these findings, OMP-GCaMP6s mice exhibited an increase in the percentage of glomeruli responding to each odorant in our panel when a 10-fold higher concentration was

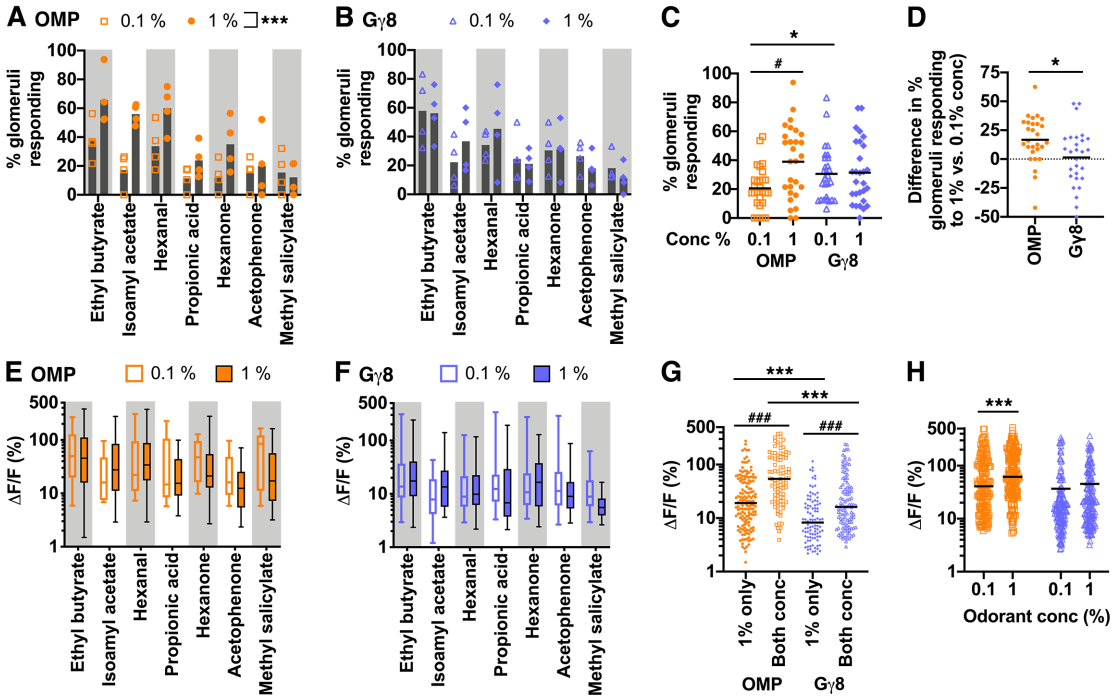

Figure 3. Immature OSNs respond to lower odorant concentrations but encode concentration less strongly than mature OSNs.

A. Greater percentage of glomeruli respond to 1% than 0.1% odorant in OMP-GCaMP6s mice (Two-way ANOVA. Effect of concentration: $P < 0.001$, $F_{1,42} = 17.9$. Effect of odorant: $P < 0.001$, $F_{6,42} = 8.31$. Interaction: $P = 0.11$, $F_{6,42} = 1.89$. n = 4 mice per group). Bars: median, data points: values for individual mice. Gray shaded areas are shown to aid visualisation only. **B.** Similar percentage of glomeruli respond to 0.1% and 1% odorant in Gγ8-GCaMP6s mice (Two-way ANOVA. Effect of concentration: $P = 0.74$, $F_{1,42} = 0.11$. Effect of odorant: $P < 0.001$, $F_{6,42} = 6.55$. Interaction: $P = 0.67$, $F_{6,42} = 0.68$. n = 4 mice per group). Bars: median, data points: values for individual mice. **C.** Greater percentage of glomeruli respond to 0.1% odorant in Gγ8-GCaMP6s than in OMP-GCaMP6s mice (One-way ANOVA. $P = 0.001$, $F_{3,108} = 6.17$. Sidak's multiple comparisons. OMP 0.1% vs. Gγ8 0.1%: $P = 0.028$, $t = 2.62$. OMP 1% vs. Gγ8 1%: $P = 0.24$, $t = 1.57$. n = 28 mouse-odorant pairs per group). Bars: median, data points: mouse-odorant pairs. **D.** Difference in percentage glomeruli responding to 1% vs. 0.1% odorant concentration is greater in OMP-GCaMP6s mice (mean: +16.7%) than in Gγ8-GCaMP6s mice (mean: +1.45%. t-test. $P = 0.015$, $t = 2.51$. n = 28 mouse-odorant pairs per group). Bars: median, symbols: mouse odorant pairs. **E.** Odorant response amplitude in OMP-GCaMP6s mice is similar for 0.1% and 1% odorants across all glomeruli (Two-way ANOVA. Effect of concentration: $P = 0.34$, $F_{1,363} = 0.89$. Effect of odorant: $P = 0.003$, $F_{6,363} = 3.43$. Interaction: $P = 0.36$, $F_{6,363} = 1.10$. n = 12-32 responding glomeruli per 0.1% odorant and 12-55 responding glomeruli per 1% odorant). Box: quartiles, whiskers: range. **F.** Odorant response amplitude in Gγ8-GCaMP6s mice is similar for 0.1% and 1% odorant concentrations across all glomeruli (Two-way ANOVA. Effect of concentration: $P = 0.66$, $F_{1,361} = 0.20$. Effect of odorant: $P = 0.021$, $F_{6,361} = 2.53$. Interaction: $P = 0.93$, $F_{6,361} = 0.32$. n = 12-46 responding glomeruli per 0.1% odorant and 13-50 responding glomeruli per 1% odorant). Box: quartiles, whiskers: range. **G.** Response amplitudes are smaller in glomeruli that respond only to 1% odorant than in those that respond to both odorant concentrations (One-way ANOVA on Ranks. $P < 0.001$, Kruskal-Wallis statistic = 88.3. Dunn's multiple comparisons. OMP respond to 1% (n = 150) vs. respond to both (n = 89): $P < 0.001$, $Z = 5.62$. Gγ8 respond to 1% (n = 95) vs. respond to both (n = 108): $P < 0.001$, $Z = 3.99$. OMP vs. Gγ8 respond to 1% odorant: $P < 0.001$, $Z = 4.79$. OMP vs. Gγ8 respond to both: $P < 0.001$, $Z = 5.72$). Bars: median, symbols: individual glomerulus-odorant pairs. **H.** For glomeruli that respond to both concentrations of individual odorants, amplitudes of responses to the 1% concentration are significantly greater in OMP-GCaMP6s mice but not in Gγ8-GCaMP6s mice (Two-way repeated measures ANOVA. Effect of genotype: $P < 0.001$, $F_{1,340} = 39.66$. Effect of concentration: $P < 0.001$, $F_{1,340} = 17.75$. Interaction: $P = 0.049$, $F_{1,340} = 3.888$. Sidak's multiple comparisons. OMP 0.1% vs. 1% concentration: $P < 0.001$, $t = 4.44$. Gγ8 0.1% vs. 1% concentration: $P = 0.22$, $t = 1.56$). Bars: mean, symbols: glomerulus-odor pairs.

delivered (Fig. 3A). In contrast, the percentage of glomeruli responding to 0.1% and 1% dilutions of each odorant was similar in Gγ8-GCaMP6s mice (Fig. 3B). To compare dilutions of each odorant was similar in Gγ8-GCaMP6s mice (Fig. 3B). To compare generalized effects of odorant concentration across genotypes, we analyzed mouse-odorant pairs. Surprisingly, a greater percentage of glomeruli responded to 0.1% odorant dilutions in Gγ8-GCaMP6s than in OMP-GCaMP6s mice (Fig. 3C), indicating that immature OSNs may detect lower concentration odorants. However, the difference in the percentage of responsive glomeruli between odorant concentrations was significantly higher in OMP-GCaMP6s mice than in Gγ8-GCaMP6s mice (Fig. 3D), consistent with the odorant-specific analysis (Fig. 3A,B), suggesting that mature OSNs can better discriminate between odorant concentrations in this range.

We also compared the amplitudes of responses evoked by the two odorant concentrations. Across the population of imaged glomeruli that responded to each odorant, response amplitudes were similar for 0.1% and 1% dilutions in both OMP-GCaMP6s and Gγ8-GCaMP6s mice (Fig. 3E,F). This was surprising, given that previous studies have found that higher odorant concentrations evoke larger amplitude glomerular responses (Johnson and Leon, 2000; Meister and Bonhoeffer, 2001; Rubin and Katz, 1999; Wachowiak and Cohen, 2001). However, we reasoned that glomeruli that responded to the 0.1% dilution of an odorant would respond more strongly to the 1% dilution of the same odorant, whereas response amplitudes may be lower for glomeruli that responded only to the 1% dilution. Indeed, in both OMP-GCaMP6s and Gγ8-GCaMP6s mice, responses to the 1% odorant dilution were larger for glomeruli that responded to both concentrations than for glomeruli that responded only to the 1% dilution (Fig. 3G). Notably, the larger response amplitude in OMP-GCaMP6s vs. Gγ8-GCaMP6s mice that we had observed previously (Fig. 1F) was evident whether comparing glomeruli that responded to both odorant concentrations or only to the 1% dilution (Fig. 3G). We further analyzed responses in glomeruli that responded to both concentrations of an odorant. We found that responses were larger to the 1% vs. the 0.1% dilution in OMP-GCaMP6s mice, but not in Gγ8-GCaMP6s mice (Fig. 3H). Overall we concluded that, at least within the concentration range that we tested, relative to mature OSNs, immature

OSNs have a lower concentration threshold, such that a larger proportion of glomeruli in Gγ8-GCaMP6s mice respond at a lower concentration, but are less effective in encoding the concentration of an odorant stimulus.

Immature OSNs form monosynaptic connections with excitatory OB neurons

In order to provide sensory information to the OB, immature OSNs must not only detect and transduce odorant binding but also transmit this information to OB neurons. We have shown previously that optogenetic stimulation of immature OSNs elicits robust stimulus-locked firing in OB neurons *in vivo* (Cheetham et al., 2016). However, we did not determine which OB neurons receive direct monosynaptic input from immature OSNs. To address this question, we performed OB slice electrophysiology using P18 – P24 Gγ8-ChIEF-Citrine and OMP-ChIEF-Citrine mice, in which the blue light-activated cation channel ChIEF fused to the yellow fluorescent protein Citrine is expressed selectively in immature and mature OSNs, respectively (Cheetham et al., 2016) (Fig. 4A). We then made whole-cell recordings of external tufted cell (ETC) and mitral cell (MC) responses to multiglomerular optogenetic stimulation (Fig. 4B). ETCs and MCs close to glomeruli innervated by ChIEF-Citrine expressing axons were selected for recording, and monosynaptic responses were isolated by including tetrodotoxin (TTX) and 4-aminopyridine (4-AP) in the recording bath (Fig. 4C). All ETCs responded to optogenetic stimulation of mature OSN axons, consistent with established ETC input patterns (Hayar et al., 2004; Vaaga and Westbrook, 2016), whereas only a subset of ETCs responded to immature OSN axon photoactivation (Fig. 4D). A subset of recorded MCs also responded to optogenetic stimulation in both Gγ8-ChIEF-Citrine and OMP-ChIEF-Citrine mice (Fig. 4E). This is consistent with the weaker monosynaptic input to MCs vs. tufted cells reported previously (Bourne and Schoppa, 2017; Gire et al., 2012; Najac et al., 2011; Vaaga and Westbrook, 2016). Response amplitudes tended to be smaller in Gγ8-ChIEF mice than in OMP-ChIEF-Citrine mice, although the small number of responding neurons precluded statistical analysis (Fig. 4F). For a subset of recorded neurons, we confirmed that responses were glutamatergic as they were completely abolished by bath application of NBQX and APV.

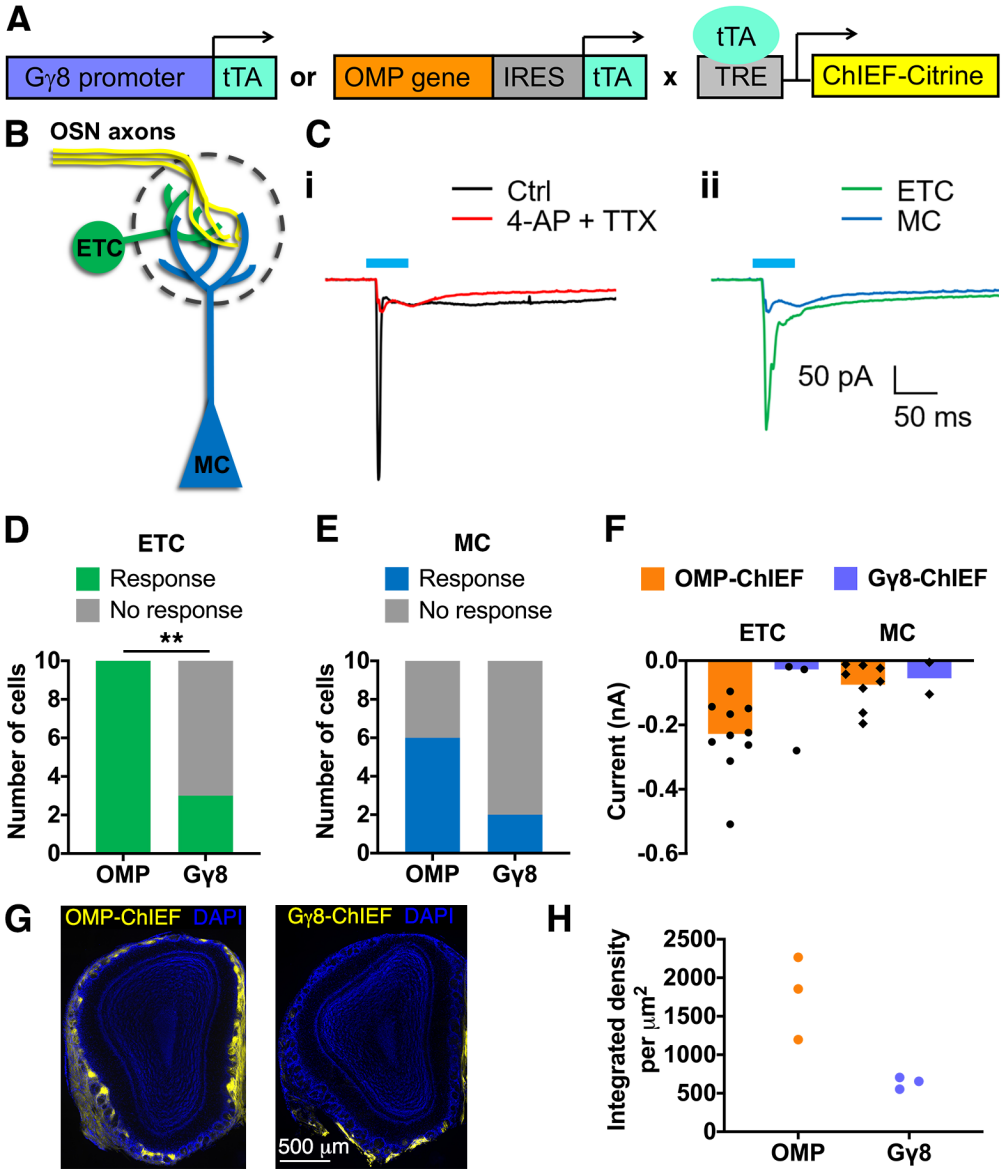

Figure 4. Immature OSNs provide monosynaptic input to external tufted and mitral cells. A. Schematic of breeding strategy to generate mice expressing ChIEF-Citrine in either immature or mature OSNs under control of the Gγ8 or OMP promoter, respectively, using the tetracycline transactivator system. **B.** Schematic of relevant OB glomerular circuitry. Whole cell voltage-clamp recordings were made from ETCs and MCs in either Gγ8-ChIEF-Citrine or OMP-ChIEF-Citrine mice. **C.** Example responses elicited by 50 ms light pulses in a Gγ8-ChIEF-Citrine mouse. **i.** Recordings from a MC made in normal ACSF (Ctrl) and in ACSF containing 1 μM TTX and 100 μM 4-AP demonstrating the presence of monosynaptic input from immature OSN axons. **ii.** Monosynaptic responses in an ETC and a MC elicited by photoactivation of immature OSN axons. All traces are averages of 50 trials. **D.** A smaller proportion of ETCs respond monosynaptically to photoactivation in Gγ8-ChIEF-Citrine vs. OMP-ChIEF-Citrine mice (Fisher's exact test. P = 0.003, n = 10 cells from 4 mice per group). **E.** A similar proportion of MCs respond monosynaptically to photoactivation in Gγ8-ChIEF-Citrine and OMP-ChIEF-Citrine mice (Fisher's exact test. P = 0.17, n = 10 cells from 4 mice per group). **F.** Amplitudes of monosynaptic responses in ETCs and MCs in Gγ8-ChIEF-Citrine and OMP-ChIEF-Citrine mice. Bars: median. Symbols: values for individual neurons. **G.** Widefield fluorescence images showing ChiEF-Citrine-expressing axons in Gγ8-ChIEF-Citrine and OMP-ChIEF-Citrine mice. **H.** Integrated density of Citrine fluorescence per μm^2 of the glomerular layer in Gγ8-ChIEF-Citrine and OMP-ChIEF-Citrine mice (n = 3 per group). Symbols: values for individual mice.

To investigate the reasons underlying the smaller proportion of ETCs that responded to optogenetic stimulation and tendency towards smaller response amplitudes in Gγ8-ChIEF-Citrine mice, we quantified the density of innervation by axons expressing ChIEF-Citrine throughout the glomerular layer in both mouse lines (Fig. 4G). Citrine fluorescence intensity was lower in the glomerular layer of all three Gγ8-ChIEF-Citrine mice than in any of the OMP-ChIEF-Citrine mice (Fig. 4H), suggesting that our multiglomerular stimulation protocol photoactivated fewer immature than mature OSN axons. Nonetheless, our data provide clear evidence that immature OSNs form monosynaptic glutamatergic connections with both ETCs and MCs.

Mice can detect odors using sensory input only from immature OSNs

Having shown that immature OSNs provide odor information to OB neurons, we next asked whether mice can detect odors using immature OSNs alone. To answer this question, we first generated mice that lacked mature OSNs. Methimazole (MMZ) selectively ablates all OSNs but spares OE basal stem cells, enabling OSNs to repopulate the OE over about a month (Bergman et al., 2002; Bergström et al., 2003; Kikuta et al., 2015; Sakamoto et al., 2007). We reasoned that at early time points after MMZ administration, the OE would contain immature but not mature OMP+ OSNs (Kikuta et al., 2015). To validate this model, we performed histological analysis of the dorsal septal OE at 3 – 7 days after MMZ administration. OE width and the number of immature GAP43+ OSNs increased linearly from 3 – 7 days post-MMZ (Fig. 5A-D). In contrast, OMP+ OSNs were completely absent at 3 – 6 days post-MMZ (Fig. 5E). At 7 days post-MMZ, two of the three mice still lacked OMP+ OSNs while the third had very sparse OMP+ OSNs: 2.6 per mm (Fig. 5E). This equates to only 0.48% of the mean OMP+ OSN density in saline-injected mice, whereas GAP43+ OSN density recovered to 55.9% of the saline-injected value by 7 days post-MMZ. Hence, we concluded that early time points post-MMZ provide an opportunity to study immature OSN function in isolation.

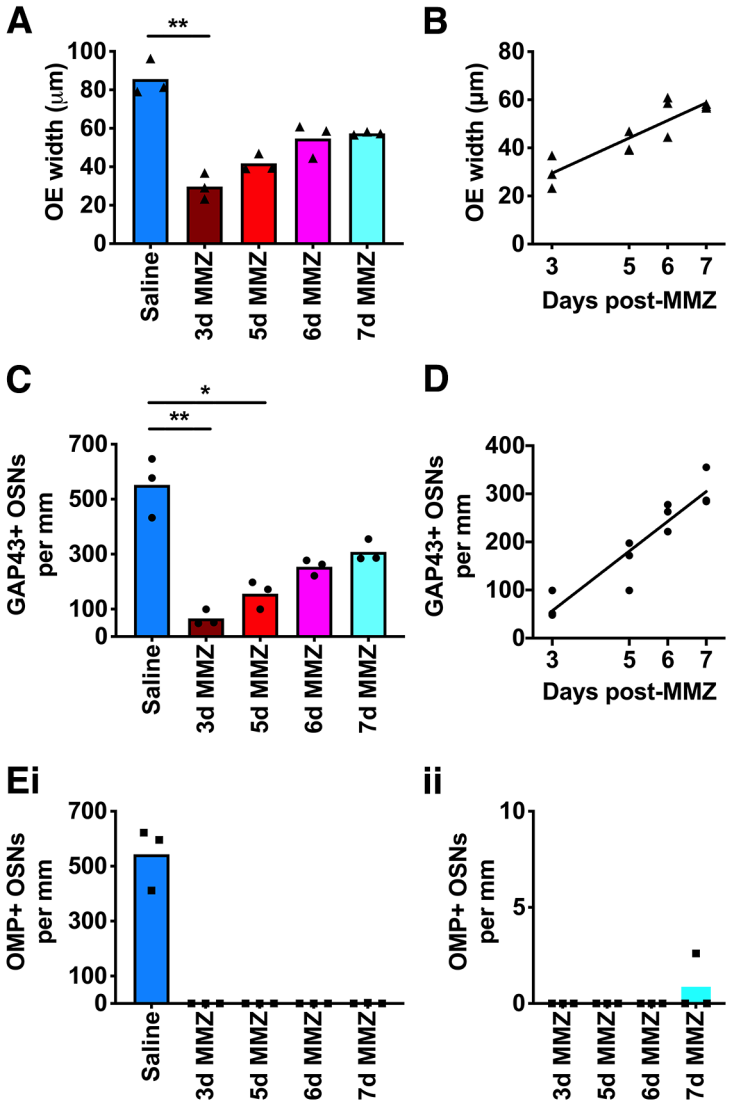

Figure 5. The olfactory epithelium contains immature but not mature OSNs at early time points after methimazole administration

A. OE width is significantly reduced 3 days post-MMZ compared to saline-injected mice (One-way ANOVA on Ranks. $P < 0.001$, Kruskal-Wallis statistic = 12.4. Dunn's multiple comparisons tests. 3-day, $P = 0.004$, $Z = 3.29$; 5d, $P = 0.071$, $Z = 2.37$; 6d, $P = 0.94$, $Z = 1.19$; 7d, $P = 0.68$, $Z = 1.37$; vs. saline. n = 3 mice per group). **B.** OE width increases linearly between 3 and 7 days post-MMZ (Linear regression. $R^2 = 0.80$, $P < 0.001$, n = 3 mice per group). **C.** Linear density of GAP43+ OSNs is significantly reduced at 3 and 5 days post-MMZ compared to saline-injected mice (One-way ANOVA on Ranks: $P < 0.001$, Kruskal-Wallis statistic = 13.4. Dunn's multiple comparisons tests. 3d MMZ, $P = 0.005$, $Z = 3.24$; 5d MMZ, $P = 0.048$, $Z = 2.51$; 6d MMZ, $P = 0.40$, $Z = 1.65$; 7d MMZ, $P = 1.00$, $Z = 0.82$; vs. saline-injected mice. n = 3 mice per group). **D.** Linear density of GAP43+ OSNs increases linearly between 3 and 7 days post-MMZ (Linear regression. $R^2 = 0.88$, $P < 0.001$, n = 3 mice per group). **E.** OMP+ OSNs are absent from the septal OE at 3-6 days post-MMZ and very sparse at 7 days post-MMZ. Note different y-axis scales in i and ii. **A-E.** Bars: mean values per group, symbols: values for individual mice.

We then performed several behavioral assays to determine whether mice can use sensory input from immature OSNs to detect and/or discriminate odors. 8-week-old mice

received a single intraperitoneal injection of either MMZ or saline and recovered for 3 – 7 days (Fig. 6A). The buried food assay tests the ability of mice to detect volatile odorants (Yang and Crawley, 2009). All saline-injected mice successfully located the buried food within 10 minutes, whereas all mice failed the task 3 days post-MMZ (Fig. 6B). As early as 5 days post-MMZ, however, 2/6 mice successfully located the buried food (Fig. 6B), and an even larger proportion located the food at 6 days (4/6 mice) and 7 days (8/12 mice) post-MMZ. Failure to locate the buried food could not be attributed to any difference in digging behavior between mice that passed or failed the task (Fig. 6C).

As an independent test of odor detection ability, we used an odor preference assay to determine whether mice could detect a food odorant (peanut butter cookie). Saline-injected mice all showed a preference for the food odorant relative to mineral oil, whereas no mice showed a preference 3 days post-MMZ (Fig. 6D,E). Just 5 days post-MMZ, however, 3/6 mice showed a significant odor preference, directly paralleling the recovery of olfactory-guided behavior in the buried food test at this time point (Fig. 6B). The proportion of mice showing a significant odor preference increased to 4/6 at 6 days and 5/6 at 7 days post-MMZ (Fig. 6D). Furthermore, preference ratio was significantly greater at 5, 6 and 7 days post-MMZ than at 3 days post-MMZ (Fig. 6E). Together, the data from these assays demonstrate that mice can detect odors using immature OSNs alone.

To determine whether sensory input from immature OSNs was sufficient to enable odor discrimination, we performed an odor habituation-dishabituation task, which quantifies the time spent sniffing a series of odorized cotton swabs (Yang and Crawley, 2009). As expected, saline-injected mice sniffed less (habituated) to familiar odorants and sniffed more (dishabituated) to a novel odorant (Fig. 6F). At 3 days post-MMZ, mice showed little habituation or dishabituation, and both parameters were significantly different to saline-injected mice (Fig. 6F-H). At 5 –7 days post-MMZ, both habituation and dishabituation began to recover, such that there was no longer a statistically significant difference from saline-injected mice across all odorants. In particular, at 6 days post-MMZ, mice showed substantial recovery of both habituation and dishabituation to 3/4 odorants tested. Hence, odor discrimination begins to recover prior to the emergence of mature OSNs.

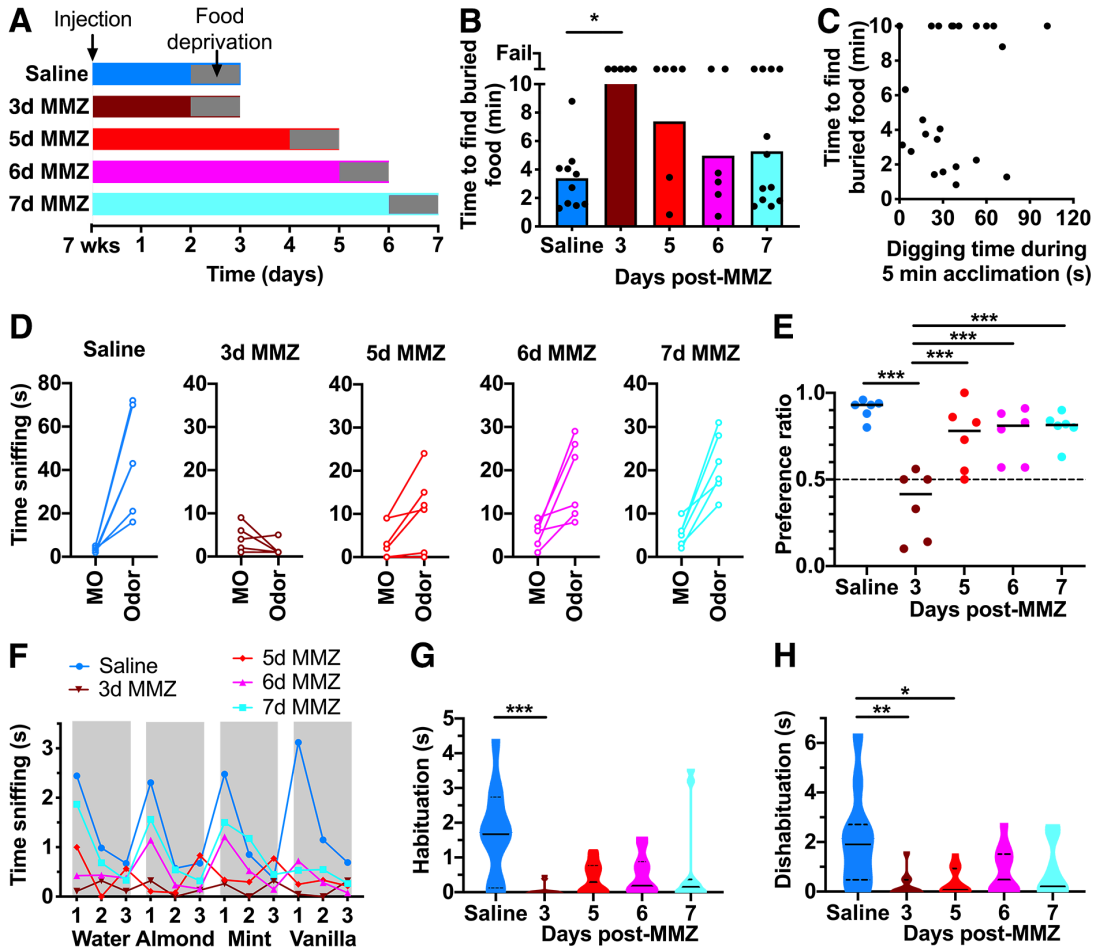

Figure 6. Mice can detect odors using only immature OSNs.
A. Experimental design for behaviour assays. Mice received an i.p. injection of MMZ or saline and were food deprived for 24 h prior to beginning the behavior assays. **B.** All mice failed to detect the buried food at 3 days post-MMZ; food detection behaviour then gradually improved with increasing time post-MMZ (One-way ANOVA on Ranks. P = 0.037, Kruskal-Wallis statistic = 10.2. Dunn's multiple comparisons tests. 3d MMZ, P = 0.011, Z = 3.00, n = 6; 5d MMZ, P = 0.26, Z = 1.84, n = 6; 6d MMZ, P = 1.00, Z = 0.76, n = 6; 7d MMZ, P = 1.00, Z = 1.08, n = 12; all vs. saline, n = 10). Bars: mean per group. Filled circles: values for individual mice. **C.** No correlation between time spent digging during habituation period and time to find buried food (Linear regression. R^2 = 0.012, P = 0.60, n = 24). **D.** Time spent sniffing mineral oil (MO) vs. Nutter Butter (Odor) for mice injected with saline or MMZ. MO and Odor values for individual mice are linked by solid lines. **E.** Preference ratio is significantly higher in saline, 5d MMZ, 6d MMZ and 7d MMZ mice than in 3d MMZ mice (One-way ANOVA. P < 0.001, F4,26 = 11.96. Sidak's multiple comparisons test. Vs. saline: 3d MMZ, P < 0.001, t = 6.43; 5d MMZ, P = 0.20, t = 1.88; 6d MMZ, P = 0.20, t = 1.73; 7d MMZ, P = 0.23, t = 1.24. Vs. 3d MMZ: 5d MMZ, P < 0.001, t = 4.54; 6d MMZ, P < 0.001, t = 4.70; 7d MMZ, P < 0.001, t = 5.18). **F.** Mean time spent sniffing each odorant swab for odor habituation-dishabituation assay (n = 11 mice per group). **G.** Habituation time across all odorants is significantly lower at 3 days post-MMZ but not at later time points (One-way ANOVA on Ranks. P = 0.004, Kruskal-Wallis statistic = 15.3. Dunn's multiple comparisons tests. 3d MMZ, P < 0.001, Z = 3.84; 5d MMZ, P = 0.070, Z = 2.38; 6d MMZ, P = 0.21, Z = 1.94; 7d MMZ, P = 0.061, Z = 2.43; vs. saline. n = 11 mice per group). Solid lines: median. Dashed lines: quartiles**. H.** Dishabituation time across all odorants is significantly lower at 3 and 5 days post-MMZ but not at later time points (One-way ANOVA on Ranks. P = 0.020, Kruskal-Wallis statistic = 11.7. Dunn's multiple comparisons test. 3d MMZ, P = 0.005, Z = 3.23; 5d MMZ, P = 0.041, Z = 2.57; 6d MMZ, P = 0.39, Z = 1.65; 7d MMZ, P = 0.31, Z = 1.76; vs. saline. n = 11 mice per group]. E,F. Solid lines: median. Dashed lines: quartiles.

Discussion

Our goal in this study was to determine what role, if any, OSNs play in odor processing before they reach maturity. Our data demonstrate that OSNs begin to provide odor input to OB neurons while they are still immature. Crucially, immature and mature OSNs had similar odorant selectivity. However, the concentration dependence of *in vivo* odorant responses differed between immature and mature OSNs. We also employed a pharmacological OSN ablation model to show that mice are able to perform behavioral odor detection tasks using sensory input derived only from immature OSNs. Our study suggests that immature OSNs play a previously unappreciated role in olfaction by providing odor input that is functionally distinct from that supplied by mature OSNs. More broadly, our findings provide new insight into the mechanisms by which endogenously generated adult-born neurons wire into existing circuits without disrupting their function.

Odorant-selective input from immature OSNs

Our slice electrophysiology experiments (Fig. 4) demonstrate that immature OSNs provide monosynaptic input to both ETCs and MCs. This finding corroborates and extends our previous *in vivo* evidence that immature OSN activation evokes robust stimulus-locked firing of neurons in multiple OB layers (Cheetham et al., 2016). Furthermore, our *in vivo* calcium imaging data demonstrate that immature OSNs can both detect odorant binding and transduce this signal to generate action potentials that propagate to the OB to elicit axon terminal calcium influx (Fig. 1). Hence, our study provides the first direct demonstration that immature OSNs provide odor input to OB neurons. This capability is consistent with key findings from recent expression analysis studies. First, immature (GAP43- or Gγ8-expressing) OSNs express ORs (Hanchate et al., 2015; Iwema and Schwob, 2003; Tan et al., 2015), with OR expression at both the mRNA and the protein level beginning at 4 days of neuronal age (Rodriguez-Gil et al., 2015), several days prior to the onset of OMP expression (Kondo et al., 2010; Liberia et al., 2019; Miragall and Graziadei, 1982; Rodriguez-Gil et al., 2015; Savya et al., 2019). Second, some immature OSNs express transcripts encoding the signal transduction machinery required for odorant binding to trigger action potential generation (Hanchate et al., 2015). Finally, 5-day-old OSNs generated in young adult mice expressed adenylyl

cyclase 3 (AC3) protein (Liberia et al., 2019), which is necessary for olfactory-dependent behavior (Wong et al., 2000).

We also found that the odorant selectivity of immature OSN responses was similar to that of their mature counterparts (Fig. 2). This is surprising, given that single cell RNA sequencing studies have indicated that a subset of immature OSNs, including some “late immature” OSNs that possess transcripts for odorant signal transduction machinery, transcribe multiple OR genes (Hanchate et al., 2015; Tan et al., 2015). If these immature OSNs also express multiple ORs at the protein level, then they would be expected to respond to a larger number of odorants (Bozza et al., 2002; Malnic et al., 1999). It is also highly likely that the axons of OSNs expressing multiple OR proteins would project to ectopic locations. This is based on multiple studies showing that OSNs in which the coding sequence for one OR has been replaced with that of a second OR (“OR swap” experiments) typically form ectopic glomeruli located between the glomeruli formed by OSNs expressing each of the individual ORs (Bozza et al., 2002; Feinstein and Mombaerts, 2004; Mombaerts et al., 1996; Wang et al., 1998). However, in tagged-OR mouse lines, stray labeled axons failing to converge on the target glomerulus are not observed in adult mice (Conzelmann et al., 2001; Feinstein and Mombaerts, 2004; Mombaerts et al., 1996; Potter et al., 2001; Ressler et al., 1994; Royal and Key, 1999). Given that OR expression begins before axons reach the glomerular layer of the OB (Rodriguez-Gil et al., 2015), a subset of the labeled axons in these tagged-OR lines would be expected to be immature at any point in time. Therefore, the absence of stray axons, together with our finding that immature OSN responses are similarly odorant selective to those of their mature counterparts, suggests that the ability of immature OSNs to provide odor information to the OB does not disrupt the highly organized glomerular input map.

There are several potential explanations for the odorant-selective responses of immature OSNs that we describe. First, there may be a regulatory mechanism that prevents translation or dendritic and axonal trafficking of more than one OR. Second, low-level expression of additional ORs, as is the case for many of the multi-OR-expressing immature OSNs identified in RNA sequencing studies (Hanchate et al., 2015; Tan et al.,

2015), may have little impact on glomerular odorant responses. Given the massive convergence of OSN axons expressing each OR to form a small number of glomeruli (Bressel et al., 2016; Mombaerts et al., 1996; Ressler et al., 1994), and the large number of possible combinations of ORs that could be co-expressed (even accounting for regional bias within the OE in terms of which OR(s) are selected (Hanchate et al., 2015)), an additional OR expressed at a low level by any individual immature OSN is likely to make a tiny, perhaps even undetectable, contribution to overall odor input to a glomerulus. It is also possible that low level expression of additional ORs does not significantly perturb axon guidance: in Ubi7 mice, in which mature OSNs express both a high level of an endogenous OR and a low level of a second OR from the OMP locus, axon navigation to the glomerulus appropriate to the endogenous OR is not disrupted (Zhou and Belluscio, 2012).

Third, OSNs expressing additional ORs at levels sufficient to perturb axon guidance, such as those expressing two ORs at similar levels (Hanchate et al., 2015; Tan et al., 2015), may not survive. It is unlikely that the axons of multi-OR-expressing OSNs coalesce to form glomeruli, given both the large number of possible OR combinations and relative expression levels and the well-established finding that there are only ~2 glomeruli per OR (Feinstein and Mombaerts, 2004; Mombaerts et al., 1996; Potter et al., 2001; Zou et al., 2004). Therefore, multi-OR-expressing OSNs that project to ectopic locations are unlikely to form synaptic connections, and hence, survive (Graziadei, 1983; Schwob et al., 1992).

Finally, it is possible that our relatively small panel of known dorsal surface-activating odorants limited our ability to detect non-selective responses in Gγ8-GCaMP6s mice. We believe that this is unlikely, given that almost 50% of imaged glomeruli responded to more than one of the odorants in our panel, indicating good coverage with potential activating odorants for the dorsal surface region that we imaged. Furthermore, the low baseline standard deviation in our images enabled us to detect even weak odorant responses with $\Delta F/F$ values as low as 1.5 % for individual glomeruli. Hence, our experimental design provided the capacity to detect reduced odorant selectivity in Gγ8-GCaMP6s mice, had it been present. In summary, there are multiple mechanisms by which odorant selective

glomerular responses could be preserved despite immature OSNs expressing transcripts for multiple ORs.

Functional role of odor information provided by immature OSNs

How does the previously unidentified odor input stream provided by immature OSNs affect olfactory function? Whereas immature OSN responses are odorant selective, similar to mature OSN responses, their concentration dependence differs. A greater percentage of glomeruli responded to low concentration odorants in Gγ8-GCaMP6s mice than in OMP-GCaMP6s mice (Fig. 3C), indicating that immature OSNs are better able to detect low concentration odorant stimuli. However, across the same concentration range, immature OSN responses were less dependent on concentration than those of their mature counterparts (Fig. 3D,G,H). These differences in the concentration dependence of odorant responses in immature vs. mature OSNs could be due to greater immature OSN intrinsic excitability or reduced $GABA_B$ receptor-mediated presynaptic inhibition (McGann, 2013) at immature OSN presynaptic terminals.

In order to test whether odor input provided by immature OSNs is behaviorally relevant, we established a MMZ ablation-based model wherein mice at early time points post-MMZ possess immature but not mature OSNs (Fig. 5). Our data from two assays performed in separate cohorts of mice provide strong evidence that odor input from immature OSNs is sufficient to mediate odor detection (Fig. 6B,E). Just 5 – 6 days after MMZ administration, a subset of mice successfully performed the buried food and odor preference assays, consistent with AC3 expression in 5-day-old OSNs (Liberia et al., 2019). We also found that the ability to discriminate odors began to recover at 6 days post-MMZ. At 5 – 6 days post-MMZ, no mature OSNs were detectable in the septal OE by OMP immunohistochemistry (Fig. 5E). We did detect a very low density of mature OSNs (2.6 per mm) in just one of the three mice analyzed at 7 days post-MMZ. However, this very restricted population of mature OSNs is unlikely to account for the behavioral recovery seen at 7 days post-MMZ for several reasons. First, odor detection and discrimination ability was already present at 6 days and did not appear suddenly at 7 days post-MMZ. Second, mature OSNs were absent from the other two 7-day post-MMZ mice analyzed

Finally, this very small number of mature OSNs represents just 0.48% of the mean density of mature OSNs in our saline-injected control mice. In contrast, immature OSN density increased linearly across 3 – 7 days post-MMZ, reaching 56% of the mean saline-injected control value by 7 days post-MMZ. Hence, our data suggest that odor input from immature OSNs supports both odor detection and at least relatively simple odor discrimination.

The time course of appearance of OMP+ OSNs following MMZ treatment in this study closely matches that described previously for both the healthy mouse OE (Kondo et al., 2010; Liberia et al., 2019; Miragall and Graziadei, 1982; Rodriguez-Gil et al., 2015; Savya et al., 2019) and the mouse OE following MMZ-mediated ablation (Kikuta et al., 2015). Hence, the time course of OSN maturation following MMZ treatment is similar to that seen during constitutive OSN neurogenesis. However, in the healthy adult olfactory system, a large number of mature OSNs project to each glomerulus, meaning that while immature OSNs can provide odor input sufficient to mediate odor detection and simple odor discrimination, they need not perform this task alone. What role, then, do they play? We propose that immature OSNs provide a functionally distinct information stream to OB neurons that prioritizes odor detection over concentration discrimination. In the healthy olfactory system, therefore, immature and mature OSNs provide complementary odor information to individual glomeruli, which may be beneficial by simultaneously enabling detection of low concentration odorants and discrimination of odorant concentration respectively. However, sensory information provided by immature OSNs is likely to make the most important contribution under circumstances when few mature OSNs are present; namely, during initial wiring of glomerular circuits or during regeneration after a significant proportion of pre-existing OSNs have been lost, such as following a viral insult or the experimental administration of MMZ. The ability of immature OSNs to respond even to low concentration odorants may be important in these scenarios to enable odor-guided behaviors essential for organismal survival.

Acknowledgements

This work was supported by grants to CEJC from the National Institute on Deafness and other Communication Disorders (R03DC014788 and R01DC018516) and the Samuel

and Emma Winters Foundation. We would like to thank Alisa Pugacheva for help with preliminary analysis, and Shawn D. Burton and members of the Cheetham lab for helpful discussions.

Author Contributions

Conceptualization, J.S.H, T.K and C.E.J.C; Methodology: J.S.H, T.K and C.E.J.C; Software: B.L and C.E.J.C; Investigation: J.S.H., T.K., B.L., R.J.M., J.T.A and C.E.J.C; Formal Analysis: J.S.H and C.E.J.C; Writing - Original Draft: J.S.H and C.E.J.C; Writing - Review and Editing: J.S.H and C.E.J.C; Visualization: J.S.H and C.E.J.C; Supervision: C.E.J.C.; Project Administration: C.E.J.C.; Funding Acquisition: C.E.J.C.

Declaration of Interests

The authors declare no competing interests.

Figures

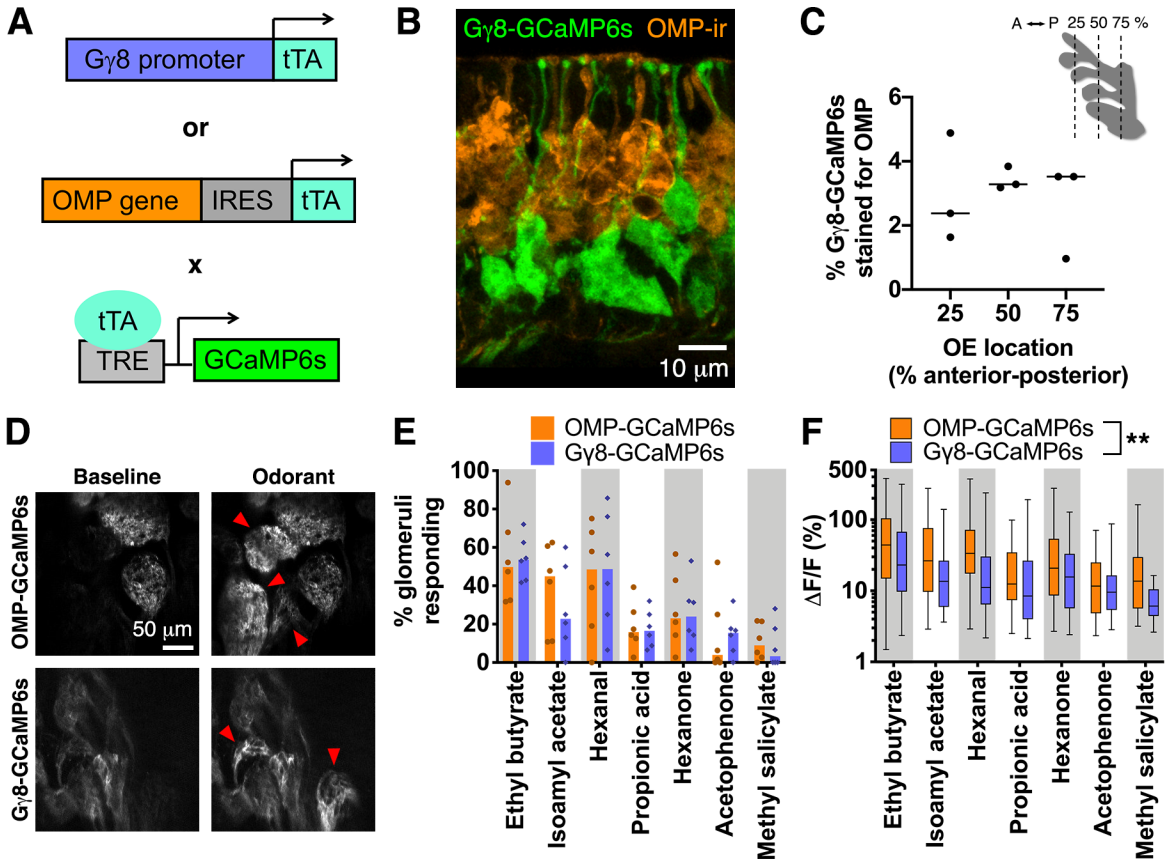

Figure 1. Immature OSNs can detect and transduce odorants.

A. Schematic of breeding strategy to generate mice expressing GCaMP6s in either immature or mature OSNs under control of the Gγ8 or OMP promoter, respectively, using the tetracycline transactivator system. **B.** Maximum intensity projection of confocal z-stack of coronal OE section from a Gγ8-GCaMP6s mouse showing lack of colocalization with OMP-stained OSNs. **C.** Co-expression of OMP in Gγ8-GCaMP6s-expressing OSNs in the septal OE along the anterior-posterior axis. Only 3.0 ± 1.2 % of Gγ8-GCaMP6s-expressing neurons co-express OMP (mean ± s.d., n = 4118 Gγ8-GCaMP6s-expressing OSNs from 3 mice). Inset shows location of analyzed OE sections. **D.** Example 2-photon images of single z-plane during single trial showing baseline fluorescence and odorant-evoked responses in OMP-GCaMP6s and Gγ8-GCaMP6s mice. Red arrows indicate ethyl butyrate-responsive glomeruli. **E.** A similar percentage of glomeruli respond to each of the 7 odorants in Gγ8-GCaMP6s vs. OMP-GCaMP6s mice (Wilcoxon signed rank test. P = 0.47, W = -10, n = 6 mice per group). Colored bars: median of 6 mice per group,

symbols: values for individual mice. Gray shaded areas are shown to aid visualisation only. **F.** Odorant-evoked responses are larger in amplitude in OMP-GCaMP6s mice vs. Gγ8-GCaMP6s mice (Two-way ANOVA. Effect of genotype: P = 0.003, $F_{1,568}$ = 8.87. Effect of odorant: P < 0.001, $F_{6,568}$ = 7.42. Interaction: P = 0.36, $F_{6,568}$ = 1.10. n = 21-87 responding glomeruli per odorant for OMP-GCaMP6s and 16-78 responding glomeruli per odorant for Gγ8-GCaMP6s). Boxes: quartiles. Whiskers: range.

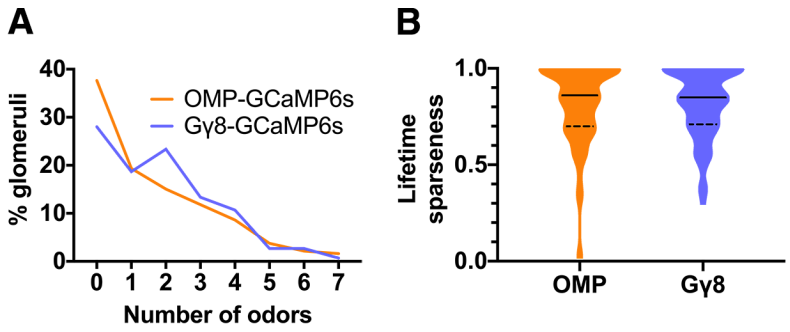

Figure 2. Immature and mature OSN axons show equivalent odorant selectivity.

A. Glomeruli in OMP-GCaMP6s and Gγ8-GCaMP6s mice respond to a similar number of odorants in a seven-odorant panel (Wilcoxon signed rank test: P = 0.95, W = -2, n = 186 glomeruli in 6 OMP-GCaMP6s mice and 150 glomeruli in 6 Gγ8-GCaMP6s mice). **B.** Violin plot showing similar lifetime sparseness of glomerular odorant responses in Gγ8-GCaMP6s and OMP-GCaMP6s mice (Kolmogorov-Smirnov test: P = 1.00, D = 0.049. n = 120 responding glomeruli in 6 OMP-GCaMP6s mice and 97 responding glomeruli in 6 Gγ8-GCaMP6s mice). Solid lines: median. Dashed lines: quartiles. Upper quartiles are at 1 and so not shown.

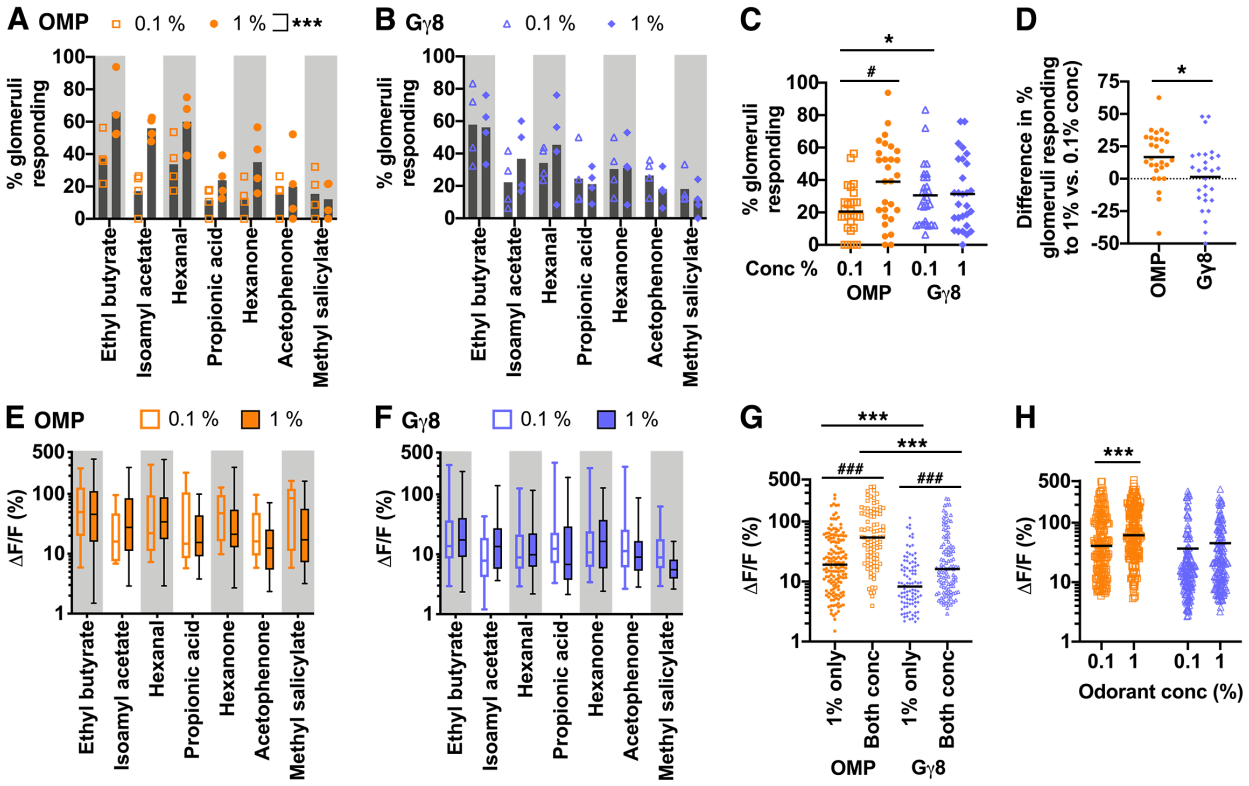

Figure 3. Immature OSNs respond to lower odorant concentrations but encode concentration less strongly than mature OSNs.

A. Greater percentage of glomeruli respond to 1% than 0.1% odorant in OMP-GCaMP6s mice (Two-way ANOVA. Effect of concentration: $P < 0.001$, $F_{1,42} = 17.9$. Effect of odorant: $P < 0.001$, $F_{6,42} = 8.31$. Interaction: $P = 0.11$, $F_{6,42} = 1.89$. n = 4 mice per group). Bars: median, data points: values for individual mice. Gray shaded areas are shown to aid visualisation only. **B.** Similar percentage of glomeruli respond to 0.1% and 1% odorant in Gγ8-GCaMP6s mice (Two-way ANOVA. Effect of concentration: $P = 0.74$, $F_{1,42} = 0.11$. Effect of odorant: $P < 0.001$, $F_{6,42} = 6.55$. Interaction: $P = 0.67$, $F_{6,42} = 0.68$. n = 4 mice per group). Bars: median, data points: values for individual mice. **C.** Greater percentage of glomeruli respond to 0.1% odorant in Gγ8-GCaMP6s than in OMP-GCaMP6s mice (One-way ANOVA. $P = 0.001$, $F_{3,108} = 6.17$. Sidak's multiple comparisons. OMP 0.1% vs. Gγ8 0.1%: $P = 0.028$, $t = 2.62$. OMP 1% vs. Gγ8 1%: $P = 0.24$, $t = 1.57$. n = 28 mouse-odorant pairs per group). Bars: median, data points: mouse-odorant pairs. **D.** Difference in percentage glomeruli responding to 1% vs. 0.1% odorant concentration is greater in OMP-GCaMP6s mice (mean: +16.7%) than in Gγ8-GCaMP6s mice (mean: +1.45%. t-test. $P = 0.015$, $t = 2.51$. n = 28 mouse-odorant pairs per group). Bars: median, symbols:

mouse odorant pairs. **E.** Odorant response amplitude in OMP-GCaMP6s mice is similar for 0.1% and 1% odorants across all glomeruli (Two-way ANOVA. Effect of concentration: $P = 0.34$, $F_{1,363} = 0.89$. Effect of odorant: $P = 0.003$, $F_{6,363} = 3.43$. Interaction: $P = 0.36$, $F_{6,363} = 1.10$. n = 12-32 responding glomeruli per 0.1% odorant and 12-55 responding glomeruli per 1% odorant). Box: quartiles, whiskers: range. **F.** Odorant response amplitude in Gγ8-GCaMP6s mice is similar for 0.1% and 1% odorant concentrations across all glomeruli (Two-way ANOVA. Effect of concentration: $P = 0.66$, $F_{1,361} = 0.20$. Effect of odorant: $P = 0.021$, $F_{6,361} = 2.53$. Interaction: $P = 0.93$, $F_{6,361} = 0.32$. n = 12-46 responding glomeruli per 0.1% odorant and 13-50 responding glomeruli per 1% odorant). Box: quartiles, whiskers: range. **G.** Response amplitudes are smaller in glomeruli that respond only to 1% odorant than in those that respond to both odorant concentrations (One-way ANOVA on Ranks. $P < 0.001$, Kruskal-Wallis statistic = 88.3. Dunn's multiple comparisons. OMP respond to 1% (n = 150) vs. respond to both (n = 89): $P < 0.001$, $Z = 5.62$. Gγ8 respond to 1% (n = 95) vs. respond to both (n = 108): $P < 0.001$, $Z = 3.99$. OMP vs. Gγ8 respond to 1% odorant: $P < 0.001$, $Z = 4.79$. OMP vs. Gγ8 respond to both: $P < 0.001$, $Z = 5.72$). Bars: median, symbols: individual glomerulus-odorant pairs. **H.** For glomeruli that respond to both 0.1% and 1% concentrations of individual odorants, amplitudes of responses to the 1% concentration are significantly greater in OMP-GCaMP6s mice but not in Gγ8-GCaMP6s mice (Two-way repeated measures ANOVA. Effect of genotype: $P < 0.001$, $F_{1,340} = 39.66$. Effect of concentration: $P < 0.001$, $F_{1,340} = 17.75$. Interaction: $P = 0.049$, $F_{1,340} = 3.888$. Sidak's multiple comparisons. OMP 0.1% vs. 1% concentration: $P < 0.001$, $t = 4.44$. Gγ8 0.1% vs. 1% concentration: $P = 0.22$, $t = 1.56$). Bars: mean, symbols: individual glomerulus-odorant pairs.

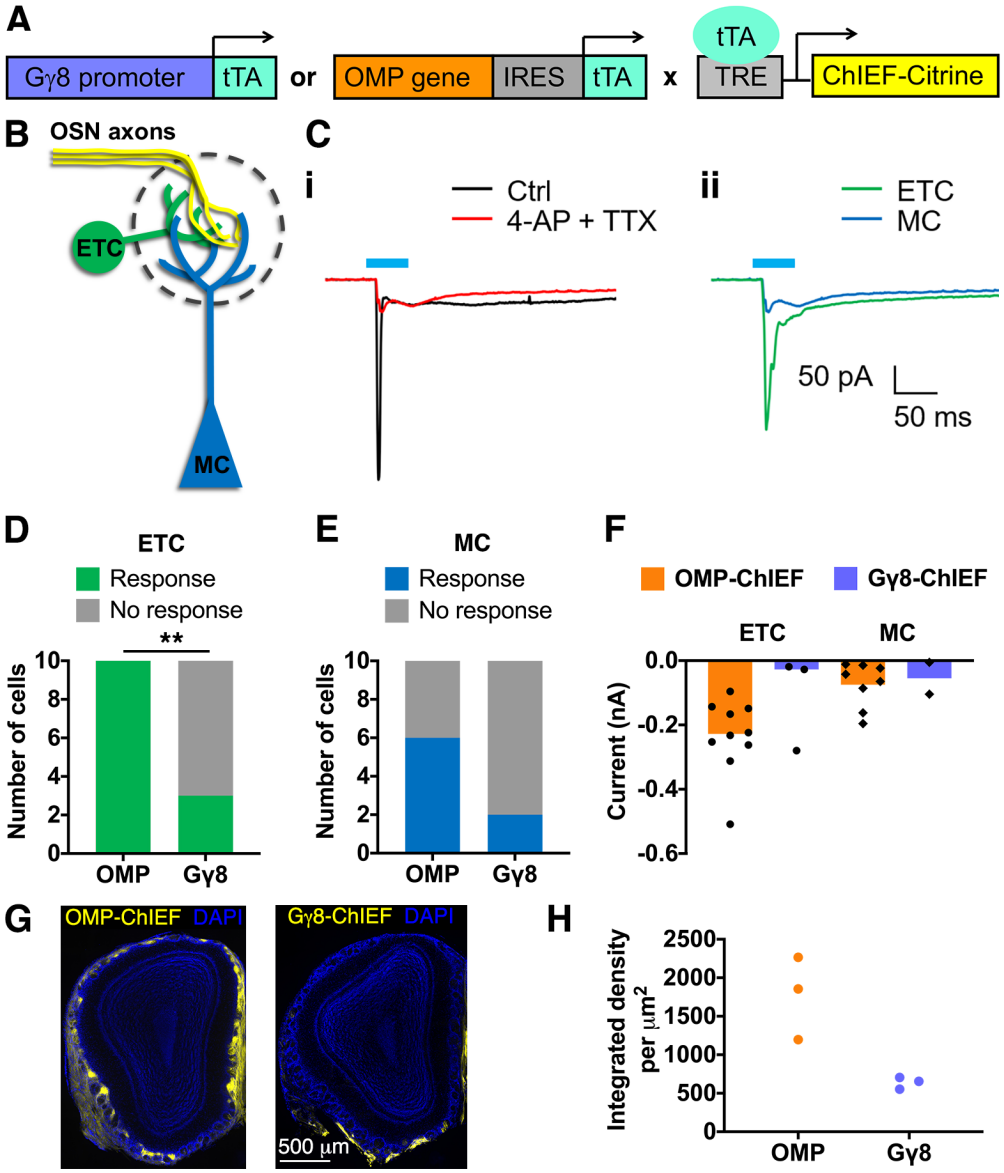

Figure 4. Immature OSNs provide monosynaptic input to external tufted and mitral cells. A. Schematic of breeding strategy to generate mice expressing ChIEF-Citrine in either immature or mature OSNs under control of the Gγ8 or OMP promoter, respectively, using the tetracycline transactivator system. **B.** Schematic of relevant OB glomerular circuitry. Whole cell voltage-clamp recordings were made from ETCs and MCs in either Gγ8-ChIEF-Citrine or OMP-ChIEF-Citrine mice. **C.** Example responses elicited by 50 ms light pulses in a Gγ8-ChIEF-Citrine mouse. **i.** Recordings from a MC made in normal ACSF (Ctrl) and in ACSF containing 1 µM TTX and 100 µM 4-AP demonstrating the presence of monosynaptic input from immature OSN axons. **ii.** Monosynaptic responses

in an ETC and a MC elicited by photoactivation of immature OSN axons. All traces are averages of 50 trials. **D.** A smaller proportion of ETCs respond monosynaptically to photoactivation in Gγ8-ChIEF-Citrine vs. OMP-ChIEF-Citrine mice (Fisher's exact test. P = 0.003, n = 10 cells from 4 mice per group). **E.** A similar proportion of MCs respond monosynaptically to photoactivation in Gγ8-ChIEF-Citrine and OMP-ChIEF-Citrine mice (Fisher's exact test. P = 0.17, n = 10 cells from 4 mice per group). **F.** Amplitudes of monosynaptic responses in ETCs and MCs in Gγ8-ChIEF-Citrine and OMP-ChIEF-Citrine mice. Bars: median. Symbols: values for individual neurons. **G.** Widefield fluorescence images showing ChiEF-Citrine-expressing axons in Gγ8-ChIEF-Citrine and OMP-ChIEF-Citrine mice. **H.** Integrated density of Citrine fluorescence per μm^2 of the glomerular layer in Gγ8-ChIEF-Citrine and OMP-ChIEF-Citrine mice (n = 3 per group). Symbols: values for individual mice.

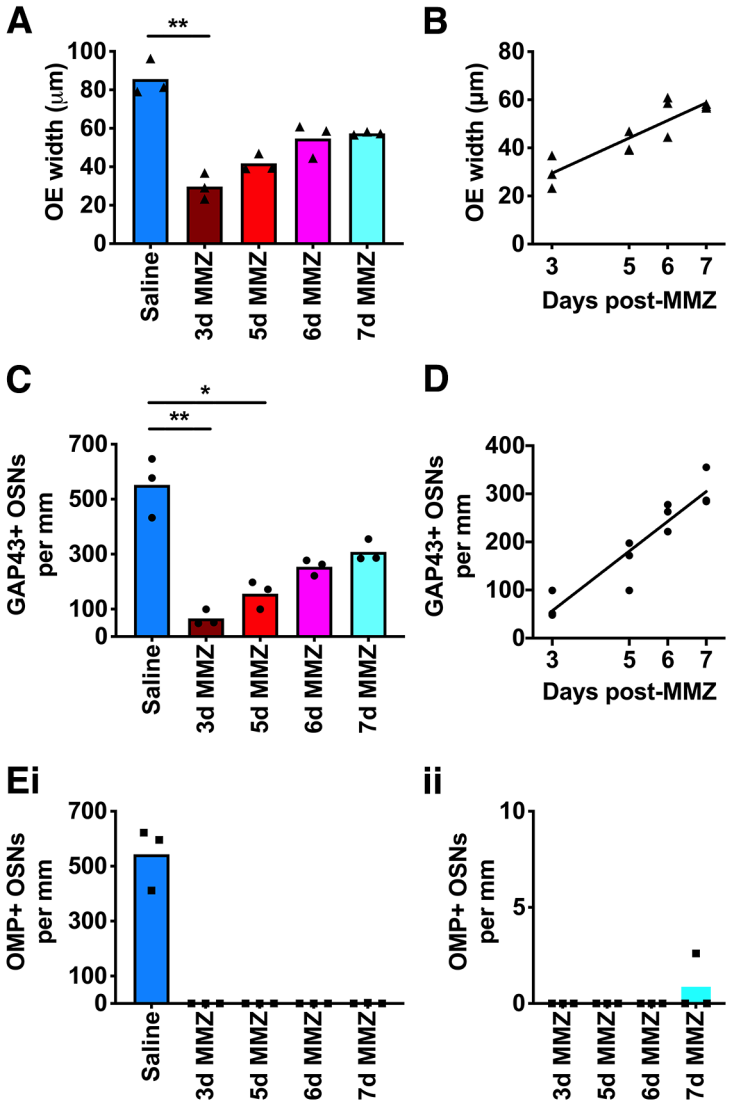

Figure 5. The olfactory epithelium contains immature but not mature OSNs at early time points after methimazole administration

A. OE width is significantly reduced 3 days post-MMZ compared to saline-injected mice (One-way ANOVA on Ranks. P < 0.001, Kruskal-Wallis statistic = 12.4. Dunn's multiple comparisons tests. 3-day, P = 0.004, Z = 3.29; 5d, P = 0.071, Z = 2.37; 6d, P = 0.94, Z = 1.19; 7d, P = 0.68, Z = 1.37; vs. saline. n = 3 mice per group). **B.** OE width increases linearly between 3 and 7 days post-MMZ (Linear regression. R^2 = 0.80, P < 0.001, n = 3 mice per group). **C.** Linear density of GAP43+ OSNs is significantly reduced at 3 and 5 days post-MMZ compared to saline-injected mice (One-way ANOVA on Ranks: P < 0.001, Kruskal-Wallis statistic = 13.4. Dunn's multiple comparisons tests. 3d MMZ, P = 0.005, Z = 3.24; 5d MMZ, P = 0.048, Z = 2.51; 6d MMZ, P = 0.40, Z = 1.65; 7d MMZ, P = 1.00, Z

= 0.82; vs. saline-injected mice. n = 3 mice per group). **D.** Linear density of GAP43+ OSNs increases linearly between 3 and 7 days post-MMZ (Linear regression. $R^2 = 0.88$, $P < 0.001$, n = 3 mice per group). **E.** OMP+ OSNs are absent from the septal OE at 3-6 days post-MMZ and very sparse at 7 days post-MMZ. Note different y-axis scales in i and ii. **A-E.** Bars: mean values per group, symbols: values for individual mice.

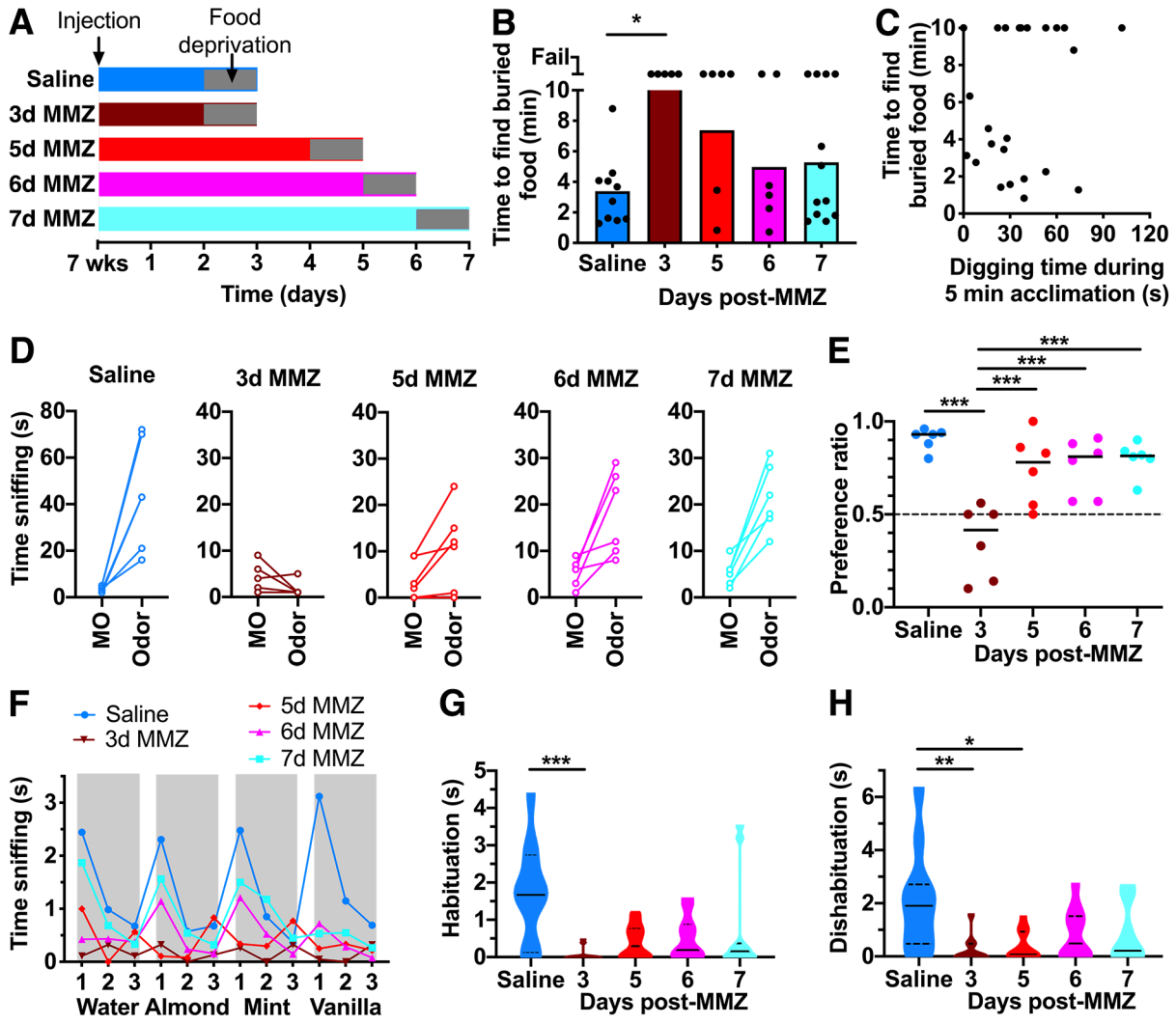

Figure 6. Mice can detect odors using only immature OSNs.

A. Experimental design for behaviour assays. Mice received an i.p. injection of MMZ or saline and were food deprived for 24 h prior to beginning the behavior assays. **B.** All mice failed to detect the buried food at 3 days post-MMZ; food detection behaviour then gradually improved with increasing time post-MMZ (One-way ANOVA on Ranks. P = 0.037, Kruskal-Wallis statistic = 10.2. Dunn's multiple comparisons tests. 3d MMZ, P = 0.011, Z = 3.00, n = 6; 5d MMZ, P = 0.26, Z = 1.84, n = 6; 6d MMZ, P = 1.00, Z = 0.76, n = 6; 7d MMZ, P = 1.00, Z = 1.08, n = 12; all vs. saline, n = 10). Bars: mean per group. Filled circles: values for individual mice. **C.** No correlation between time spent digging during habituation period and time to find buried food (Linear regression. R^2 = 0.012, P = 0.60, n = 24). **D.** Time spent sniffing mineral oil (MO) vs. Nutter Butter (Odor) for mice

injected with saline or MMZ. MO and Odor values for individual mice are linked by solid lines. **E.** Preference ratio is significantly higher in saline, 5d MMZ, 6d MMZ and 7d MMZ mice than in 3d MMZ mice (One-way ANOVA. $P < 0.001$, $F_{4,26} = 11.96$. Sidak's multiple comparisons test. Vs. saline: 3d MMZ, $P < 0.001$, $t = 6.43$; 5d MMZ, $P = 0.20$, $t = 1.88$; 6d MMZ, $P = 0.20$, $t = 1.73$; 7d MMZ, $P = 0.23$, $t = 1.24$. Vs. 3d MMZ: 5d MMZ, $P < 0.001$, $t = 4.54$; 6d MMZ, $P < 0.001$, $t = 4.70$; 7d MMZ, $P < 0.001$, $t = 5.18$). **F.** Mean time spent sniffing each odorant swab for odor habituation-dishabituation assay (n = 11 mice per group). **G.** Habituation time across all odorants is significantly lower at 3 days post-MMZ but not at later time points (One-way ANOVA on Ranks. $P = 0.004$, Kruskal-Wallis statistic = 15.3. Dunn's multiple comparisons tests. 3d MMZ, $P < 0.001$, $Z = 3.84$; 5d MMZ, $P = 0.070$, $Z = 2.38$; 6d MMZ, $P = 0.21$, $Z = 1.94$; 7d MMZ, $P = 0.061$, $Z = 2.43$; vs. saline. n = 11 mice per group). Solid lines: median. Dashed lines: quartiles**. H.** Dishabituation time across all odorants is significantly lower at 3 and 5 days post-MMZ but not at later time points (One-way ANOVA on Ranks. $P = 0.020$, Kruskal-Wallis statistic = 11.7. Dunn's multiple comparisons test. 3d MMZ, $P = 0.005$, $Z = 3.23$; 5d MMZ, $P = 0.041$, $Z = 2.57$; 6d MMZ, $P = 0.39$, $Z = 1.65$; 7d MMZ, $P = 0.31$, $Z = 1.76$; vs. saline. n = 11 mice per group]. E,F. Solid lines: median. Dashed lines: quartiles.

Methods

Experimental animals

All animal procedures conformed to National Institutes of Health guidelines and were approved by the Carnegie Mellon University and University of Pittsburgh Institutional Animal Care and Use Committees. C57BL/6J mice (strain #000664) were purchased from the Jackson Laboratory and all other lines were bred in-house. Mice were maintained on a 12 h light/dark cycle in individually ventilated cages with unrestricted access to food and water unless otherwise stated. Mice were group-housed where same sex littermates were available, unless otherwise stated. A total of 122 mice were used in this study.

Generation of the Gγ8-tTA (Nguyen et al., 2007), OMP-IRES-tTA (Yu et al., 2004), tetO-ChIEF-Citrine (Cheetham et al., 2016), tetO-GCaMP6s (Wekselblatt et al., 2016), OMP-

Cre (Li et al., 2004) and Ai9 (Madisen et al., 2009) mouse lines has been described previously. Mice for 2-photon calcium imaging experiments were Gγ8-GCaMP6s [Gγ8-tTA$^{+/-}$;tetO-GCaMP6s$^{+/-}$] or OMP-GCaMP6s [OMP-tTA$^{+/-}$;tetO-GCaMP6s$^{+/-}$]. Mice for electrophysiology experiments were Gγ8-ChIEF-Citrine [Gγ8-tTA$^{+/-}$;tetO-ChIEF-Citrine$^{+/-}$] or OMP-ChIEF-Citrine [OMP-tTA$^{+/-}$;tetO-ChIEF-Citrine$^{+/-}$]. Mice for behavioral experiments were C57BL/6J (The Jackson Laboratory), Gγ8-ChIEF-Citrine [Gγ8-tTA$^{+/-}$;tetO-ChIEF-Citrine$^{+/-}$] or OMP-tdT [OMP-Cre$^{+/-}$;Ai9$^{+/-}$]. All genetically modified mice were of mixed 129 x C57BL/6J background, and each experimental group comprised approximately equal numbers of male and female mice, which were randomly assigned to experimental groups. Mice were genotyped by PCR using the primers described previously (Cheetham et al., 2016; Li et al., 2004; Madisen et al., 2009; Wekselblatt et al., 2016).

2-photon calcium imaging and data analysis

P21-23 mice were anesthetized with ketamine/xylazine (100/10 mg/kg), ketoprofen (5 mg/kg) was administered and ~1 mm diameter craniotomies were made over one or both OBs for each mouse as described (Cheetham et al., 2016). A head bar was also attached. Mice were imaged with either a VIVO 2-photon microscope (3i) using a Plan-Apo 20x/1.0NA water-immersion objective (Zeiss) and a Chameleon Ultra II IR laser (Coherent) mode-locked at 935 nm using SlideBook (3i); or a Bergamo II 2-photon microscope (ThorLabs) using a SemiApo 20x/1.0NA water-immersion objective (Olympus) and an Insight X3 IR laser (Newport) mode-locked at 935 nm using ThorImage 4.0 (ThorLabs). Time-lapse images of a single optical section were collected at 10.17 frames/s on the VIVO system (266 μm^2, pixel size 1.04 μm) or 15 frames/s on the Bergamo system (328 μm^2, pixel size 0.64 μm). Top-up doses of ketamine/xylazine (50/5 mg/kg) were given during the imaging session as required to maintain light anesthesia.

Odorant stimulation was performed using a custom-built Arduino-controlled olfactometer. Stimulation and image acquisition timing were controlled and recorded using either Igor Pro (Wavemetrics) or Python, ThorSync and ThorImage (ThorLabs). The seven-odorant panel consisted of odorants known to activate the dorsal surface of the OB: ethyl butyrate,

hexanal, 2-hexanone, propionic acid, isoamyl acetate, methyl salicylate and acetophenone (all 1% v/v dilutions in mineral oil, except for concentration experiments, in which 1% and 0.1% v/v dilutions were compared). Saturated vapor from odorant vials, or a blank stimulus consisting of deodorized dehumidified air, were delivered into an oxygen carrier stream at a constant flow rate of 1 l/min. The air puff stimulus used to test for putative mechanosensory responses consisted of a 1 s deodorized dehumidified air puff delivered at a flow rate of 1 l/min in the absence of a carrier stream. All stimuli were 1 s in duration and were delivered via a tube positioned 5 mm from the opening of the external nares. All image trials were 20 s in duration (4 s baseline, 1 s stimulus, 15 s post-stimulus). Three trials were collected for each stimulus, with odorants and blank stimuli delivered in a pseudo-random order with 90 s between trials.

Data were analyzed using Fiji (ImageJ) (Schindelin et al., 2012). For each imaged region of interest, glomeruli were manually outlined, and the same outlines were used for analysis of all stimulus presentations. Mean fluorescence intensity over time was extracted for each glomerulus for each trial. Data from the three trials were then averaged for each stimulus. The fluorescence intensity change (ΔF) was calculated as the difference between a 1 s baseline prior to stimulus onset and the peak fluorescence within 3 s after stimulus onset. A glomerulus was defined as responding to a stimulus if the ΔF amplitude was greater than three standard deviations of the baseline period. $\Delta F/F$ (%) was reported as (baseline – peak)/baseline x 100 for significant responses only. For blank subtraction, the $\Delta F/F$ in response to the blank (deodorized air) stimulus for a glomerulus was subtracted from the $\Delta F/F$ in response to each odorant.

Lifetime sparseness (S_L) provides a measure of the degree to which a glomerular response was attributable entirely to one odorant (highly selective, $S_L = 1$) versus equally distributed across all odorants ($S_L = 0$). S_L was calculated as $(1-(\Sigma_{i=1,n}(r_i/n)^2)/(\Sigma_{i=1,n}(r_i^2/n)))/(1-1/n)$, where r_i is the $\Delta F/F$ of the glomerular response to odorant i and n is the total number of odorants (Poo and Isaacson, 2009). The difference in percentage of glomeruli responding to 1% vs. 0.1% odorant was calculated by subtracting the percentage responding to the 0.1% dilution from the percentage responding to the 1%

dilution for each mouse-odorant pair.

Slice electrophysiology and optogenetic stimulation

P18-24 Gγ8-ChIEF-Citrine and OMP-ChIEF-Citrine were deeply anesthetized with isoflurane and decapitated into ice-cold oxygenated artificial cerebrospinal fluid (ACSF). The olfactory bulbs were dissected, and sagittal slices (310 μm thick) were prepared using a vibratome (VT1200S; Leica). Slices recovered in ACSF at 37°C for 30 min. ACSF contained (in mM): 125 NaCl, 25 glucose, 2.5 KCl, 25 $NaHCO_3$, 1.25 NaH_2PO_4, 1 $MgCl_2$, and 2.5 $CaCl_2$. Slices were then incubated in ACSF at room temperature until recording. Slices were continuously superfused in ACSF at 35°C while recording. As in our previous *in vivo* study, recordings were targeted to the ventral OB, which exhibits robust innervation by immature OSN axons at this age (Cheetham et al., 2016). Voltage-clamp recordings were made using electrodes filled with (in mM): 135 KCl, 10 HEPES, 10 Na-phosphocreatine, 3 Mg-ATP, 0.3 Na_3GTP, and 0–0.025 Alexa Fluor 594. Whole-cell patch-clamp recordings were made using a Multiclamp 700A amplifier (Molecular Devices) and an ITC-18 acquisition board (Instrutech) controlled by Igor Pro (WaveMetrics). Mitral cells (MCs) and external tufted cells (ETCs) were identified under IR-DIC by shape and location in olfactory bulb laminae. Pharmacological agents used were the voltage-gated Na^+ channel antagonist tetrodotoxin (TTX, 1 μM), the voltage-gated K^+ channel antagonist 4-aminopyridine (4-AP, 100 μM), the NMDA receptor antagonist DL-2-amino-5-phosphonovaleric acid (APV, 20 μM), and the AMPA receptor antagonist 2,3-dihydroxy-6-nitro-7-sulfamoyl-benzo(F)quinoxaline (NBQX, 10 μM). Cells were only included for analysis if their holding current at -70 mV was less than -300 pA. MCs and ETCs close to glomeruli innervated by ChIEF-Citrine expressing axons were selected for recording. At least 10 minutes elapsed between cell selection and the start of photoactivation experiments. For photoactivation of immature or mature OSN axons, slices were illuminated (50 ms light pulse) by a 75W xenon arc lamp passed through a YFP excitation filter and 60x/0.9NA water-immersion objective (Olympus) centered on the glomerular layer. An open field stop was used to enable multiglomerular activation. Monosynaptic light-evoked EPSCs were isolated in the presence of TTX and 4-AP, and 50 trials per cell were recorded. Sequential recordings in normal ACSF and in the

presence of TTX and 4-AP were performed for a subset of cells. APV and NBQX were applied at the end of a subset of recordings to confirm that the recorded responses were glutamatergic. For analysis, the mean baseline over a 100 ms window before stimulus onset was subtracted from the recorded current trace. EPSC peak amplitude was defined as the most negative value of the baseline-subtracted current trace in a 100 ms window after stimulus onset for each trial. A cell was classified as having a monosynaptic response if the EPSC peak amplitude exceeded three standard deviations of the pre-stimulus baseline current.

Methimazole ablation of olfactory sensory neurons

8-week-old Gγ8-ChIEF-Citrine, OMP-tdT and C57BL6/J mice received a single intraperitoneal injection of either methimazole (MMZ; 75 mg/kg in sterile saline) or an equivalent volume of saline. Behavioral assays were conducted 3 – 7 d later. Time points were accurate to ± 1 h at the start of the behavioral assay(s).

Odor detection and discrimination assays

A buried food assay (Yang and Crawley, 2009) and an odor preference assay (Pankevich et al., 2004) were used to test odor detection and an odor habituation-dishabituation assay (Yang and Crawley, 2009) was used to test odor discrimination. Mice were transported to the behavioral testing room at least 30 min prior to commencing the assay(s). All trials were videoed. 8-week-old Gγ8-ChIEF-Citrine and OMP-tdT mice performed the buried food and/or habituation-dishabituation assays (6 mice per group performed the two assays consecutively). Mice were singly housed, and food deprived for 24 h prior to the assays. Each mouse that performed the buried food assay received a single Froot Loop (Kelloggs) for odorant familiarization at the start of food deprivation. All mice consumed this Froot Loop. For the buried food assay each mouse had 5 min to acclimate to the test cage, which contained 3 cm corn cob bedding. Time digging during this 5 min session was quantified from videos. The mouse was then briefly removed, a Froot Loop was buried near the center of the cage, and the mouse was returned to the test cage. The time to locate the buried Froot Loop was then measured; mice failed the task if they had not located the buried food within 10 min. For the odor habituation-

dishabituation assay each mouse acclimated for 30 min in the test cage, which contained a dry cotton swab attached to the lid. Mice were then presented with a series of odorant-soaked swabs, each attached to the cage lid, for 2 min each. The time spent sniffing each swab (scored as nose oriented toward, and within 1 inch of, the swab) was recorded. The odorant series consisted of 3 trials each of water, almond, mint and vanilla, presented in a fixed order. These are neutral odorants that elicit only modest levels of sniffing (Crawley et al., 2007; Wersinger et al., 2007). Odorants were food extracts diluted 1:100 in water. Habituation was quantified as the difference in sniffing time between the first and second trial with each odorant. Dishabituation was quantified as the difference in sniffing time between the final trial of an odorant and the first trial of the subsequent odorant. Three mice that had completed both assays underwent transcardial perfusion (see next section) immediately after completing behavioral testing.

A separate group of 8-week-old C57BL/6J mice performed the odor preference assay. Male and female mice were housed in groups of three. For two consecutive days, each mouse was transferred to a clean cage and given 1.5 g Nutter Butter cookie (Nabisco). Mice were returned to their home cage once they had eaten the cookie. The next day, mice received a saline or MMZ injection. Mice were food deprived for 16 hours prior to odor preference testing, which occurred 3 – 7 d after saline or MMZ injection. Each mouse was transferred to a test cage and given 10 min to acclimate. Mice then had 10 minutes to investigate filter paper squares odorized with mineral oil (MO) or Nutter Butter cookie suspended in mineral oil (Odor). Mice could not make direct contact with the filter paper squares. The total time spent sniffing each filter paper square was scored manually from videos. Preference ratio was calculated as the time sniffing Odor divided by the total time spent sniffing Odor plus MO, i.e., a value of 0.5 indicates no preference. A preference ratio of 0.75 (i.e. duration sniffing Odor was three times that sniffing MO) was defined as indicating a significant odor preference.

Perfusion, immunohistochemistry and image analysis

Transcardial perfusion, preparation and immunohistochemical staining of OB and OE sections were performed exactly as described previously (Cheetham et al., 2016). All sections were mounted with Vectashield containing DAPI (Vector Labs).

Citrine fluorescence was quantified for 3 OB sections per mouse (left and right OBs at 25%, 50% and 75% along the anterior-posterior axis) for Gγ8-ChIEF-Citrine and OMP-ChIEF-Citrine mice (n = 3 per group). Images (pixel size 0.64 μm) of entire sections were collected using an Eclipse 90i large area-scanning widefield microscope equipped with a Plan-Apo 10x/ 0.45NA air objective and Elements software (Nikon). Camera settings were the same for all images. Total integrated fluorescence intensity in the Citrine channel was normalized to the area of the glomerular layer for each section using Fiji.

To quantify co-expression of OMP in Gγ8-GCaMP6s-expressing OSNs, OE sections (3 per mouse at 25%, 50% and 75% along the anterior-posterior axis) were stained to detect OMP (anti-OMP primary antibody [1:5000, 96h at 4°C, catalog #544-10001, Wako Chemicals] and donkey anti-goat-Alexa Fluor 546 secondary antibody [1:500, 1h at room temperature]), and GCaMP6s (GFP-Booster-Atto-488 [1:500, 1h at room temperature, gba-488-100, Chromotek]). Confocal z-stacks of ~1mm of dorsal septal OE were collected (voxel size, 0.13 x 0.13 x 0.5 μm) using an A1R confocal microscope equipped with an Apo 60x/1.4NA oil immersion objective and Elements software (Nikon). Numbers of Gγ8-GCaMP6s+ and Gγ8-GCaMP6s+/OMP+ OSNs were quantified and the percentage of Gγ8-GCaMP6s+/OMP+ OSNs determined in each section for three mice.

For histological analysis in MMZ- and saline-injected mice, OE sections (3 per antibody per mouse at 25%, 50% and 75% along the anterior-posterior axis) were stained for GAP43 as a marker of immature OSNs (anti-GAP43 primary antibody, 1:1000 for 48h at 4°C, NB300-143, Novus Biologicals; donkey anti-rabbit-Alexa Fluor 546 secondary antibody, 1:500 for 1h at room temperature), or OMP (see above) as a marker of mature OSNs. 2-photon z-stacks of ~1mm of the dorsal septal OE were collected using the Bergamo system with 2-photon excitation at 800 nm. Image analysis was performed in

Fiji. OE width (from the basal lamina to the apical surface) was measured at 3 different locations each on the left and right sides of the OE and averaged for each section. The grand mean width for the three sections per mouse was then calculated. GAP43+ and OMP+ OSNs were counted in each image, and the mean value expressed as linear density (cells per mm) was calculated for each mouse.

Statistics

Statistical analyses were performed using Prism 8 or Prism 9 (GraphPad). Parametric tests were performed for normally distributed data with equal variances and for $\log_{10}$-transformed data that met these criteria; otherwise, non-parametric tests were performed. Fisher's exact test and Wilcoxon signed rank test were used to compare proportions of responding neurons or glomeruli. Two-tailed unpaired t-tests, Mann-Whitney rank sum tests, or Kolmogorov-Smirnov tests were used to compare two groups, whereas one-way ANOVA, one-way ANOVA on Ranks, or two-way ANOVA were used to compare multiple groups. Linear regression was used to test for relationships between factors. α was 0.05. The results of all statistical tests are reported in the figure legends.

KEY RESOURCES TABLE

REAGENT or RESOURCE	SOURCE	IDENTIFIER
Antibodies		
Goat polyclonal anti-olfactory marker protein	Wako Chemicals	#544-10001 RRID:AB_664696
Rabbit polyclonal anti-GAP43	Novus Biologicals	NB300-143 RRID:AB_10001196
Donkey anti-goat IgG (H+L) Alexa Fluor 546 conjugated	Thermo Fisher Scientific	A11056 RRID:AB_142628
Donkey anti-rabbit IgG (H+L) Alexa Fluor 546	Thermo Fisher Scientific	A10040 RRID:AB_2534016
GFP-Booster-Atto-488	Chromotek	gba-488-100 RRID:AB_2631386
Chemicals		
Ethyl butyrate	Millipore Sigma	E15791-25ML CAS: 105-54-4
Isoamyl acetate	Acros Organics	AC150662500 CAS: 123-92-2
Hexanal	Alpha Aesar	AAA1626522 CAS: 66-25-1
2-hexanone	Fluka	20270 CAS: 591-78-6
Acetophenone	Fluka	00790-250ML CAS: 98-86-2

Methyl salicylate	Millipore Sigma	M6752-250ML CAS: 119-36-8
Propionic acid	Millipore Sigma	402907-100ML CAS: 79-09-4
VECTASHIELD Antifade Mounting Medium with DAPI	Vector Labs	H-1200
Methimazole	Millipore Sigma	M8506-25G CAS: 60-56-0
Vanilla extract	McCormick	N/A
Peppermint extract	McCormick	N/A
Almond extract	McCormick	N/A
Nutter Butter cookies	Nabisco	N/A
Froot Loops	Kelloggs	N/A
Experimental Models: Organisms/Strains		
Mouse: C57BL/6J	The Jackson Laboratory	JAX:000664 RRID:IMSR_JAX:000664
Mouse: tetO-GCaMP6s B6;DBA-Tg(tetO-GCaMP6s)2Niell/J	The Jackson Laboratory	JAX:024742 RRID:IMSR_JAX:024742
Mouse: OMP-cre B6;129P2-Omptm4(cre)Mom/MomJ	The Jackson Laboratory	JAX:006668 RRID:IMSR_JAX:006668
Mouse: Ai9 B6.Cg-Gt(ROSA)26Sortm9(CAG-tdTomato)Hze/J	The Jackson Laboratory	JAX:007909 RRID:IMSR_JAX:007909
Mouse: OMP-IRES-tTA B6;129-Omptm1(tTA)Gogo/J	The Jackson Laboratory	JAX:017754, RRID:IMSR_JAX:017754
Mouse: tetO-ChIEF-Citrine	Cheetham et al. 2016	N/A
Mouse: Gγ8-tTA	Nguyen et al. 2007	N/A
Oligonucleotides		
Primers for Gγ8-tTA, OMP-IRES-tTA, tetO-ChIEF-Citrine	Cheetham et al. 2016	N/A
Primers for OMP-cre	Li et al. 2004	N/A
Primers for Ai9	Madisen et al. 2009	N/A
Primers for tetO-GCaMP6s	Wekselblatt et al. 2016	N/A
Software and Algorithms		
Fiji	Schindelin et al. (2012)	https://imagej.net/Fiji
Python	Pyzo	https://pyzo.org
Nikon Elements	Nikon	
ThorImage	ThorLabs	
SlideBook	3i	
Igor Pro	Wavemetrics	

Supplementary Figure

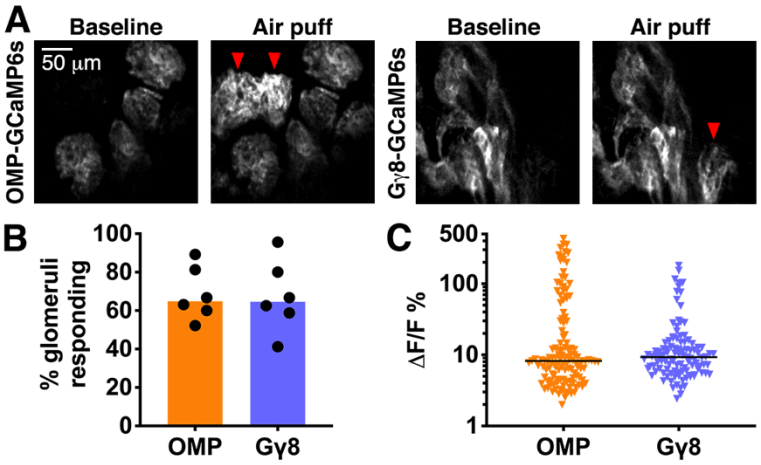

Figure S1. Immature and mature OSNs respond to a deodorized air puff stimulus. **A.** Example 2-photon images of single z-plane during single trial showing baseline and responses evoked by deodorized air puffs in OMP-GCaMP6s and Gγ8-GCaMP6s mice. Red arrows indicate air puff-responsive glomeruli. **B.** Similar percentage of glomeruli respond to air puff stimulus in OMP-GCaMP6s (median 64.9%) and Gγ8-GCaMP6s (median: 64.6%) mice (Mann-Whitney rank sum test. P = 0.85, U = 16.5, n = 6 mice per group). Bars: median, circles: values for individual mice. **C.** Similar response amplitude to air puff stimulation in OMP-GCaMP6s mice (median 8.2%, n = 131 glomeruli from 6 mice) and Gγ8-GCaMP6s mice (median 9.3%, n = 107 glomeruli from 6 mice. Mann-Whitney rank sum test. P = 0.43, U = 6593). Bars: median, symbols: values for individual glomeruli.

Supplementary Discussion

Role of putative mechanosensory input from immature OSNs

Recent studies suggest that mature OSNs can detect mechanical stimuli (Carey et al., 2009; Chen et al., 2012; Connelly et al., 2015; Grosmaitre et al., 2007; Iwata et al., 2017). Our data from mature OSN axons expressing GCaMP6s were similar to a previous *in vivo* study that described airflow responses in tracheotomized mice (Iwata et al., 2017), in terms of both the percentage of glomeruli that responded to the air puff and air puff response amplitude. The most parsimonious explanation for these data is therefore that our air puff stimulus, delivered to the external nares, also evokes mechanosensory

responses. Importantly, we show that immature OSNs also exhibit putative mechanosensory responses similar to those in mature OSNs. This is not unexpected, in the context that immature OSNs respond to odorants and that mature OSNs employ the same OR-based signal transduction machinery to generate both odorant and mechanosensory responses (Chen et al., 2012; Connelly et al., 2015). It is interesting that putative mechanosensory responses were similar in amplitude in glomeruli of Gγ8-GCaMP6s mice and OMP-GCaMP6s mice. This suggests that responses to mechanical stimuli may be present as soon as immature OSNs begin to provide OB input, and hence that airflow-induced phase coding of odor identity (Iwata et al., 2017) may also apply to sensory input received from immature OSNs. Another intriguing possibility is that mechanosensory-evoked activity could promote synapse formation and hence survival (Schwob et al., 1992) of newborn OSNs. Most newborn OSNs do not survive beyond 14 days after terminal cell division in juvenile mice (Savya et al., 2018), perhaps because they must compete with both other immature OSNs and established mature OSNs to form synapses with postsynaptic targets. The role of odor-evoked activity in promoting the survival or integration of OSNs is unclear, as many of the ORs that are expressed will never encounter an odorant ligand (Saraiva et al., 2015). In contrast, ORs are more likely to encounter mechanosensory stimuli, and a majority of glomeruli receive putative mechanosensory-evoked input (Fig. S1) (Iwata et al., 2017).

References

Bergman, U., Östergren, A., Gustafson, A.-L., and Brittebo, E. (2002). Differential effects of olfactory toxicants on olfactory regeneration. Archives of Toxicology *76*, 104–112.

Bergström, U., Giovanetti, A., Piras, E., and Brittebo, E.B. (2003). Methimazole-Induced Damage in the Olfactory Mucosa: Effects on Ultrastructure and Glutathione Levels. Toxicologic Pathology *31*, 379–387.

Blanco-Hernández, E., Valle-Leija, P., Zomosa-Signoret, V., Drucker-Colín, R., and Vidaltamayo, R. (2012). Odor memory stability after reinnervation of the olfactory bulb. PloS One *7*, e46338.

Bourne, J.N., and Schoppa, N.E. (2017). Three-dimensional synaptic analyses of mitral cell and external tufted cell dendrites in rat olfactory bulb glomeruli. J Comp Neurol *525*, 592–609.

Bozza, T., Feinstein, P., Zheng, C., and Mombaerts, P. (2002). Odorant Receptor Expression Defines Functional Units in the Mouse Olfactory System. J Neurosci *22*, 3033–3043.

Bressel, O.C., Khan, M., and Mombaerts, P. (2016). Linear correlation between the number of olfactory sensory neurons expressing a given mouse odorant receptor gene and the total volume of the corresponding glomeruli in the olfactory bulb. J Comp Neurol *524*, 199–209.

Carey, R.M., Verhagen, J.V., Wesson, D.W., Pírez, N., and Wachowiak, M. (2009). Temporal Structure of Receptor Neuron Input to the Olfactory Bulb Imaged in Behaving Rats. J Neurophysiol *101*, 1073–1088.

Cheetham, C.E., Park, U., and Belluscio, L. (2016). Rapid and continuous activity-dependent plasticity of olfactory sensory input. Nature Communications *7*, 10729.

Chen, X., Xia, Z., and Storm, D.R. (2012). Stimulation of Electro-Olfactogram Responses in the Main Olfactory Epithelia by Airflow Depends on the Type 3 Adenylyl Cyclase. J Neurosci *32*, 15769–15778.

Chess, A., Simon, I., Cedar, H., and Axel, R. (1994). Allelic inactivation regulates olfactory receptor gene expression. Cell *78*, 823–834.

Cheung, M.C., Jang, W., Schwob, J.E., and Wachowiak, M. (2014). Functional recovery of odor representations in regenerated sensory inputs to the olfactory bulb. Frontiers in Neural Circuits *7*, 207.

Clowney, E.J., Magklara, A., Colquitt, B.M., Pathak, N., Lane, R.P., and Lomvardas, S. (2011). High-throughput mapping of the promoters of the mouse olfactory receptor genes reveals a new type of mammalian promoter and provides insight into olfactory receptor gene regulation. Genome Res *21*, 1249–1259.

Connelly, T., Yu, Y., Grosmaitre, X., Wang, J., Santarelli, L.C., Savigner, A., Qiao, X., Wang, Z., Storm, D.R., and Ma, M. (2015). G protein-coupled odorant receptors underlie mechanosensitivity in mammalian olfactory sensory neurons. Proceedings of the National Academy of Sciences *112*, 590–595.

Conzelmann, S., Malun, D., Breer, H., and Strotmann, J. (2001). Brain targeting and glomerulus formation of two olfactory neuron populations expressing related receptor types. Eur J Neurosci *14*, 1623–1632.

Crawley, J.N., Chen, T., Puri, A., Washburn, R., Sullivan, T.L., Hill, J.M., Young, N.B., Nadler, J.J., Moy, S.S., Young, L.J., et al. (2007). Social approach behaviors in oxytocin knockout mice: Comparison of two independent lines tested in different laboratory environments. Neuropeptides *41*, 145–163.

Dalton, R.P., and Lomvardas, S. (2014). Chemosensory Receptor Specificity and Regulation. Annual Review of Neuroscience *38*, 331–349.

Doty, R.L., and Kamath, V. (2014). The influences of age on olfaction: a review. Frontiers in Psychology *5*, 20.

Feinstein, P., and Mombaerts, P. (2004). A Contextual Model for Axonal Sorting into Glomeruli in the Mouse Olfactory System. Cell *117*, 817–831.

Firestein, S. (2001). How the olfactory system makes sense of scents. Nature *413*, 211–218.

Forest, J., Chalençon, L., Midroit, M., Terrier, C., Caillé, I., Sacquet, J., Benetollo, C., Martin, K., Richard, M., Didier, A., et al. (2019). Role of Adult-Born Versus Preexisting Neurons Born at P0 in Olfactory Perception in a Complex Olfactory Environment in Mice. Cereb Cortex *30*, 534–549.

Gire, D.H., Franks, K.M., Zak, J.D., Tanaka, K.F., Whitesell, J.D., Mulligan, A.A., Hen, R., and Schoppa, N.E. (2012). Mitral Cells in the Olfactory Bulb Are Mainly Excited through a Multistep Signaling Path. The Journal of Neuroscience *32*, 2964–2975.

Graziadei, M.G. (1983). Experimental studies on the olfactory marker protein. III. The olfactory marker protein in the olfactory neuroepithelium lacking connections with the forebrain. Brain Research *262*, 303–308.

Graziadei, P.P., and Graziadei, G.A.M. (1978). Continuous nerve cell renewal in the olfactory system. In Development of Sensory Systems, M. Jacobson, ed. (Springer-Verlag), pp. 55–83.

Grelat, A., Benoit, L., Wagner, S., Moigneu, C., Lledo, P.-M., and Alonso, M. (2018). Adult-born neurons boost odor–reward association. Proceedings of the National Academy of Sciences 201716400.

Grosmaitre, X., Santarelli, L.C., Tan, J., Luo, M., and Ma, M. (2007). Dual functions of mammalian olfactory sensory neurons as odor detectors and mechanical sensors. Nature Neuroscience *10*, nn1856.

Hahn, C., Han, L., Rawson, N.E., Mirza, N., Borgmann-Winter, K., Lenox, R.H., and Arnold, S.E. (2005). In vivo and in vitro neurogenesis in human olfactory epithelium. Journal of Comparative Neurology *483*, 154–163.

Hanchate, N.K., Kondoh, K., Lu, Z., Kuang, D., Ye, X., Qiu, X., Pachter, L., Trapnell, C., and Buck, L.B. (2015). Single-cell transcriptomics reveals receptor transformations during olfactory neurogenesis. Science *350*, 1251–1255.

Hayar, A., Karnup, S., Ennis, M., and Shipley, M.T. (2004). External Tufted Cells: A Major Excitatory Element That Coordinates Glomerular Activity. J Neurosci *24*, 6676–6685.

Hinds, J.W., Hinds, P.L., and McNelly, N.A. (1984). An autoradiographic study of the mouse olfactory epithelium: Evidence for long-lived receptors. The Anatomical Record *210*, 375–383.

Holl, A.-M. (2018). Survival of mature mouse olfactory sensory neurons labeled genetically perinatally. Molecular and Cellular Neurosciences *88*, 258–269.

Iwata, R., Kiyonari, H., and Imai, T. (2017). Mechanosensory-Based Phase Coding of Odor Identity in the Olfactory Bulb. Neuron *96*, 1139-1152.e7.

Iwema, C.L., and Schwob, J.E. (2003). Odorant receptor expression as a function of neuronal maturity in the adult rodent olfactory system. Journal of Comparative Neurology *459*, 209–222.

Johnson, B.A., and Leon, M. (2000). Modular representations of odorants in the glomerular layer of the rat olfactory bulb and the effects of stimulus concentration. J Comp Neurology *422*, 496–509.

Kikuta, S., Sakamoto, T., Nagayama, S., Kanaya, K., Kinoshita, M., Kondo, K., Tsunoda, K., Mori, K., and Yamasoba, T. (2015). Sensory deprivation disrupts homeostatic regeneration of newly generated olfactory sensory neurons after injury in adult mice. The Journal of Neuroscience *35*, 2657–2673.

Kohli, P., Soler, Z.M., Nguyen, S.A., Muus, J.S., and Schlosser, R.J. (2016). The Association Between Olfaction and Depression: A Systematic Review. Chemical Senses *41*, 479–486.

Kondo, K., Suzukawa, K., Sakamoto, T., Watanabe, K., Kanaya, K., Ushio, M., Yamaguchi, T., Nibu, K., Kaga, K., and Yamasoba, T. (2010). Age-related changes in cell dynamics of the postnatal mouse olfactory neuroepithelium: Cell proliferation, neuronal differentiation, and cell death. Journal of Comparative Neurology *518*, 1962–1975.

Leung, C.T., Coulombe, P.A., and Reed, R.R. (2007). Contribution of olfactory neural stem cells to tissue maintenance and regeneration. Nature Neuroscience *10*, 720–726.

Li, J., Ishii, T., Feinstein, P., and Mombaerts, P. (2004). Odorant receptor gene choice is reset by nuclear transfer from mouse olfactory sensory neurons. Nature *428*, 393–399.

Li, W.L., Chu, M.W., Wu, A., Suzuki, Y., Imayoshi, I., and Komiyama, T. (2018). Adult-born neurons facilitate olfactory bulb pattern separation during task engagement. ELife *7*, e33006.

Liberia, T., Martin-Lopez, E., Meller, S.J., and Greer, C.A. (2019). Sequential maturation of olfactory sensory neurons in the mature olfactory epithelium. Eneuro *6*, ENEURO.0266-19.2019.

Lledo, P.-M.M., Alonso, M., and Grubb, M.S. (2006). Adult neurogenesis and functional plasticity in neuronal circuits. Nature Reviews Neuroscience *7*, 179–193.

Lois, C., and Alvarez-Buylla, A. (1993). Proliferating subventricular zone cells in the adult mammalian forebrain can differentiate into neurons and glia. Proc National Acad Sci *90*, 2074–2077.

Luskin, M.B. (1993). Restricted proliferation and migration of postnatally generated neurons derived from the forebrain subventricular zone. Neuron *11*, 173–189.

Mackay-Sim, A., and Kittel, P. (1991). On the Life Span of Olfactory Receptor Neurons. The European Journal of Neuroscience *3*, 209–215.

Madisen, L., Zwingman, T.A., Sunkin, S.M., Oh, S.W., Zariwala, H.A., Gu, H., Ng, L.L., Palmiter, R.D., Hawrylycz, M.J., Jones, A.R., et al. (2009). A robust and high-throughput Cre reporting and characterization system for the whole mouse brain. Nat Neurosci *13*, 133–140.

Malnic, B., Hirono, J., Sato, T., and Buck, L. (1999). Combinatorial receptor codes for odors. Cell *96*, 713–723.

McGann, J.P. (2013). Presynaptic Inhibition of Olfactory Sensory Neurons: New Mechanisms and Potential Functions. Chemical Senses *38*, 459–474.

McIntyre, J.C., Titlow, W.B., and McClintock, T.S. (2010). Axon growth and guidance genes identify nascent, immature, and mature olfactory sensory neurons. Journal of Neuroscience Research *88*, 3243–3256.

Meister, M., and Bonhoeffer, T. (2001). Tuning and Topography in an Odor Map on the Rat Olfactory Bulb. J Neurosci *21*, 1351–1360.

Miragall, F., and Graziadei, G.M. (1982). Experimental studies on the olfactory marker protein. II. Appearance of the olfactory marker protein during differentiation of the olfactory sensory neurons of mouse: an immunohistochemical and autoradiographic study. Brain Research *239*, 245–250.

Mombaerts, P., Wang, F., Dulac, C., Chao, S., Nemes, A., Mendelsohn, M., Edmondson, J., and Axel, R. (1996). Visualizing an olfactory sensory map. Cell *87*, 675–686.

Najac, M., Jan, D.D.S., Reguero, L., Grandes, P., and Charpak, S. (2011). Monosynaptic and Polysynaptic Feed-Forward Inputs to Mitral Cells from Olfactory Sensory Neurons. J Neurosci *31*, 8722–8729.

Nguyen, M.Q., Zhou, Z., Marks, C.A., Ryba, N.J.P., and Belluscio, L. (2007). Prominent Roles for Odorant Receptor Coding Sequences in Allelic Exclusion. Cell *131*, 1009–1017.

Pankevich, D.E., Baum, M.J., and Cherry, J.A. (2004). Olfactory Sex Discrimination Persists, Whereas the Preference for Urinary Odorants from Estrous Females Disappears in Male Mice after Vomeronasal Organ Removal. J Neurosci *24*, 9451–9457.

Poo, C., and Isaacson, J.S. (2009). Odor representations in olfactory cortex: “sparse” coding, global inhibition, and oscillations. Neuron *62*, 850–861.

Potter, S., Zheng, C., Koos, D., Feinstein, P., Fraser, S., and Mombaerts, P. (2001). Structure and emergence of specific olfactory glomeruli in the mouse. The Journal of Neuroscience *21*, 9713–9723.

Ressler, K., Sullivan, S., and Buck, L. (1994). Information coding in the olfactory system: evidence for a stereotyped and highly organized epitope map in the olfactory bulb. Cell *79*, 1245–1255.

Rodriguez-Gil, D.J., Bartel, D.L., Jaspers, A.W., Mobley, A.S., Imamura, F., and Greer, C.A. (2015). Odorant receptors regulate the final glomerular coalescence of olfactory sensory neuron axons. Proceedings of the National Academy of Sciences *112*, 5821–5826.

Royal, S., and Key, B. (1999). Development of P2 olfactory glomeruli in P2-internal ribosome entry site-tau-LacZ transgenic mice. The Journal of Neuroscience *19*, 9856–9864.

Rubin, B.D., and Katz, L.C. (1999). Optical Imaging of Odorant Representations in the Mammalian Olfactory Bulb. Neuron *23*, 499–511.

Ryba, N., and Tirindelli, R. (1995). A novel GTP-binding protein gamma-subunit, G gamma 8, is expressed during neurogenesis in the olfactory and vomeronasal neuroepithelia. The Journal of Biological Chemistry *270*, 6757–6767.

Sakamoto, T., Kondo, K., Kashio, A., Suzukawa, K., and Yamasoba, T. (2007). Methimazole-induced cell death in rat olfactory receptor neurons occurs via apoptosis triggered through mitochondrial cytochrome c-mediated caspase-3 activation pathway. Journal of Neuroscience Research *85*, 548–557.

Saraiva, L.R., Ibarra-Soria, X., Khan, M., Omura, M., Scialdone, A., Mombaerts, P., Marioni, J.C., and Logan, D.W. (2015). Hierarchical deconstruction of mouse olfactory sensory neurons: from whole mucosa to single-cell RNA-seq. Scientific Reports *5*, 18178.

Savya, S.P., Kunkhyen, T., and Cheetham, C. (2019). Low survival rate of young adult-born olfactory sensory neurons in the undamaged mouse olfactory epithelium. J. Bioenerg. Biomembr. *51*, 41–51.

Schindelin, J., Arganda-Carreras, I., Frise, E., Kaynig, V., Longair, M., Pietzsch, T., Preibisch, S., Rueden, C., Saalfeld, S., Schmid, B., et al. (2012). Fiji: an open-source platform for biological-image analysis. Nature Methods *9*, 676–682.

Schwob, J.E., Szumowski, K.E., and Stasky, A.A. (1992). Olfactory sensory neurons are trophically dependent on the olfactory bulb for their prolonged survival. The Journal of Neuroscience : The Official Journal of the Society for Neuroscience *12*, 3896–3919.

Schwob, J.E., Youngentob, S.L., Ring, G., Iwema, C.L., and Mezza, R.C. (1999). Reinnervation of the rat olfactory bulb after methyl bromide-induced lesion: Timing and extent of reinnervation. Journal of Comparative Neurology *412*, 439–457.

Schwob, J.E., Jang, W., Holbrook, E.H., Lin, B., Herrick, D.B., Peterson, J.N., and Coleman, J. (2017). Stem and progenitor cells of the mammalian olfactory epithelium: Taking poietic license. The Journal of Comparative Neurology *525*, 1034–1054.

Serizawa, S., Ishii, T., Nakatani, H., Tsuboi, A., Nagawa, F., Asano, M., Sudo, K., Sakagami, J., Sakano, H., Ijiri, T., et al. (2000). Mutually exclusive expression of odorant receptor transgenes. Nature Neuroscience *3*, 687–693.

Serizawa, S., Miyamichi, K., Nakatani, H., Suzuki, M., Saito, M., Yoshihara, Y., and Sakano, H. (2003). Negative Feedback Regulation Ensures the One Receptor-One Olfactory Neuron Rule in Mouse. Science *302*, 2088–2094.

Tan, L., Li, Q., and Xie, S.X. (2015). Olfactory sensory neurons transiently express multiple olfactory receptors during development. Molecular Systems Biology *11*, 844.

Tirindelli, R., and Ryba, N. (1996). The G-protein gamma-subunit G gamma 8 is expressed in the developing axons of olfactory and vomeronasal neurons. The European Journal of Neuroscience *8*, 2388–2398.

Vaaga, C.E., and Westbrook, G.L. (2016). Parallel processing of afferent olfactory sensory information. The Journal of Physiology *594*, 6715–6732.

Verhaagen, J., Oestreicher, A., Gispen, W., and Margolis, F. (1989). The expression of the growth associated protein B50/GAP43 in the olfactory system of neonatal and adult rats. J Neurosci *9*, 683–691.

Wachowiak, M., and Cohen, L.B. (2001). Representation of Odorants by Receptor Neuron Input to the Mouse Olfactory Bulb. Neuron *32*, 723–735.

Wallace, J.L., Wienisch, M., and Murthy, V.N. (2017). Development and Refinement of Functional Properties of Adult-Born Neurons. Neuron *96*, 883-896.e7.

Wang, F., Nemes, A., Mendelsohn, M., and Axel, R. (1998). Odorant receptors govern the formation of a precise topographic map. Cell *93*, 47–60.

Wekselblatt, J.B., Flister, E.D., Piscopo, D.M., and Niell, C.M. (2016). Large-scale imaging of cortical dynamics during sensory perception and behavior. J Neurophysiol *115*, 2852–2866.

Wersinger, S.R., Caldwell, H.K., Martinez, L., Gold, P., Hu, S. -B., and Young, W.S. (2007). Vasopressin 1a receptor knockout mice have a subtle olfactory deficit but normal aggression. Genes Brain Behav *6*, 540–551.

Wong, S.T., Trinh, K., Hacker, B., Chan, G.C.K., Lowe, G., Gaggar, A., Xia, Z., Gold, G.H., and Storm, D.R. (2000). Disruption of the Type III Adenylyl Cyclase Gene Leads to Peripheral and Behavioral Anosmia in Transgenic Mice. Neuron *27*, 487–497.

Yang, M., and Crawley, J.N. (2009). Simple Behavioral Assessment of Mouse Olfaction. Curr Protoc Neurosci *48*, 8.24.1-8.24.12.

Yu, C.R., Power, J., Barnea, G., O'Donnell, S., Brown, H., Osborne, J., Axel, R., and Gogos, J.A. (2004). Spontaneous Neural Activity Is Required for the Establishment and Maintenance of the Olfactory Sensory Map. Neuron *42*, 553–566.

Zhou, Z., and Belluscio, L. (2012). Coding odorant concentration through activation timing between the medial and lateral olfactory bulb. Cell Reports *2*, 1143–1150.

Zou, D.-J.J., Feinstein, P., Rivers, A.L.L., Mathews, G.A., Kim, A., Greer, C.A., Mombaerts, P., and Firestein, S. (2004). Postnatal refinement of peripheral olfactory projections. Science (New York, N.Y.) *304*, 1976–1979.